Cell

Microbiota imbalance induced by dietary sugar disrupts immune-mediated protection from metabolic syndrome

Graphical abstract

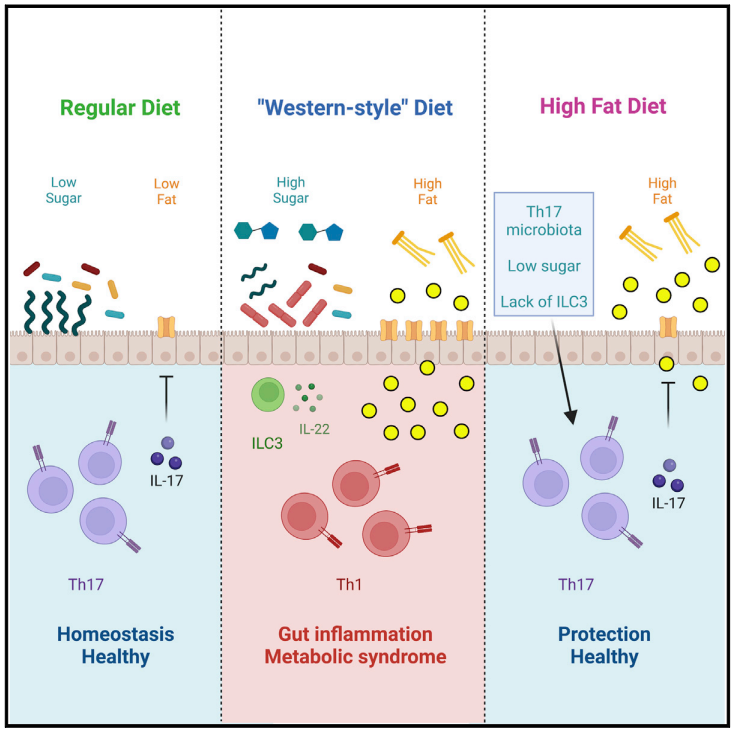

Highlights

- Commensal-induced Th17 cells regulate epithelial lipid absorption
- Sugar and ILC3 increase *Faecalibaculum rodentium* to displace Th17-inducing bacteria
- Microbiota-induced Th17 cells protect from diet-induced obesity and metabolic disease
- Sugar eliminates commensal Th17 cells to increase the risk for metabolic disease

Authors

Yoshinaga Kawano, Madeline Edwards, Yiming Huang, ..., Daniel Mucida, Kenya Honda, Ivaylo I. Ivanov

Correspondence

ii2137@cumc.columbia.edu

In brief

Sugar in mouse diets promotes metabolic disease by upsetting the gut microbial balance and driving loss of the Th17 cells that regulate lipid absorption by the intestinal epithelium.

Kawano et al., 2022, Cell *185*, 3501–3519
September 15, 2022
https://doi.org/10.1016/j.cell.2022.08.005

CellPress

Cell

CellPress

Article

Microbiota imbalance induced by dietary sugar disrupts immune-mediated protection from metabolic syndrome

Yoshinaga Kawano,[1,12] Madeline Edwards,[1,11] Yiming Huang,[2,3,11] Angelina M. Bilate,[6] Leandro P. Araujo,[1] Takeshi Tanoue,[8,9] Koji Atarashi,[8,9] Mark S. Ladinsky,[10] Steven L. Reiner,[1,5] Harris H. Wang,[3,4] Daniel Mucida,[6,7] Kenya Honda,[8,9] and Ivaylo I. Ivanov[1,13,*]

[1]Department of Microbiology and Immunology, Vagelos College of Physicians and Surgeons, Columbia University, New York, NY 10032, USA
[2]Integrated Program in Cellular, Molecular, and Biomedical Studies, Columbia University, New York, NY 10032, USA
[3]Department of Systems Biology, Vagelos College of Physicians and Surgeons, Columbia University, New York, NY 10032, USA
[4]Department of Pathology and Cell Biology, Vagelos College of Physicians and Surgeons, Columbia University, New York, NY 10032, USA
[5]Department of Pediatrics, Vagelos College of Physicians and Surgeons, Columbia University, New York, NY 10032, USA
[6]Laboratory of Mucosal Immunology, The Rockefeller University, New York, NY 10065, USA
[7]Howard Hughes Medical Institute, The Rockefeller University, New York, NY 10065, USA
[8]Department of Microbiology and Immunology, Keio University School of Medicine, Tokyo, Japan
[9]RIKEN Center for Integrative Medical Sciences, Yokohama, Japan
[10]Division of Biology and Biological Engineering, California Institute of Technology, Pasadena, CA 91125, USA
[11]These authors contributed equally
[12]Present address: Division of Endocrinology, Metabolism, and Nephrology, Department of Internal Medicine, Keio University School of Medicine, Tokyo, Japan
[13]Lead contact
*Correspondence: ii2137@cumc.columbia.edu
https://doi.org/10.1016/j.cell.2022.08.005

SUMMARY

How intestinal microbes regulate metabolic syndrome is incompletely understood. We show that intestinal microbiota protects against development of obesity, metabolic syndrome, and pre-diabetic phenotypes by inducing commensal-specific Th17 cells. High-fat, high-sugar diet promoted metabolic disease by depleting Th17-inducing microbes, and recovery of commensal Th17 cells restored protection. Microbiota-induced Th17 cells afforded protection by regulating lipid absorption across intestinal epithelium in an IL-17-dependent manner. Diet-induced loss of protective Th17 cells was mediated by the presence of sugar. Eliminating sugar from high-fat diets protected mice from obesity and metabolic syndrome in a manner dependent on commensal-specific Th17 cells. Sugar and ILC3 promoted outgrowth of *Faecalibaculum rodentium* that displaced Th17-inducing microbiota. These results define dietary and microbiota factors posing risk for metabolic syndrome. They also define a microbiota-dependent mechanism for immuno-pathogenicity of dietary sugar and highlight an elaborate interaction between diet, microbiota, and intestinal immunity in regulation of metabolic disorders.

INTRODUCTION

Obesity and metabolic syndrome are complex physiological conditions that lead to many pathologies, including cardiovascular disease, stroke, and type 2 diabetes (T2D) (Global et al., 2016). Dietary changes are a major factor for the increase in incidence of obesity and metabolic syndrome (GBD 2015, 2017; Ward et al., 2019). In both humans and mice, Western-style high-fat diet (HFD) initiates a cascade of events that ultimately result in obesity and obesity-associated metabolic complications, such as metabolic syndrome and T2D. Although much is known about later-stage pathophysiology of these conditions, the initiating events are incompletely understood. In addition, the role of non-fat dietary components is not well established. For example, whether sugar content in diets is a significant contributor to metabolic syndrome is debatable, and the mechanisms by which sugar may drive metabolic disorders are unclear (Macdonald, 2016; Stanhope, 2016). The intestine is the largest immune organ and interfaces dietary antigens with the host. The intestinal immune system has emerged as an important regulator of metabolic homeostasis (Khan et al., 2021; Winer et al., 2016). HFD has been implicated in increasing intestinal inflammation, which can contribute to endotoxemia and adipose tissue inflammation (Kawano et al., 2016; Luck et al., 2015). The mechanisms by which HFD increases intestinal inflammation, as well as the dietary components mediating these changes, have not been defined. Moreover, how mucosal immune cells affect diet-induced obesity (DIO) and metabolic syndrome is unclear.

CD4 T cells play a central role in maintaining tissue homeostasis and direct the nature of immune responses in the gut and other tissues. However, the contribution of individual T helper subsets to metabolic syndrome is less clear. T helper (Th)17 cells can promote

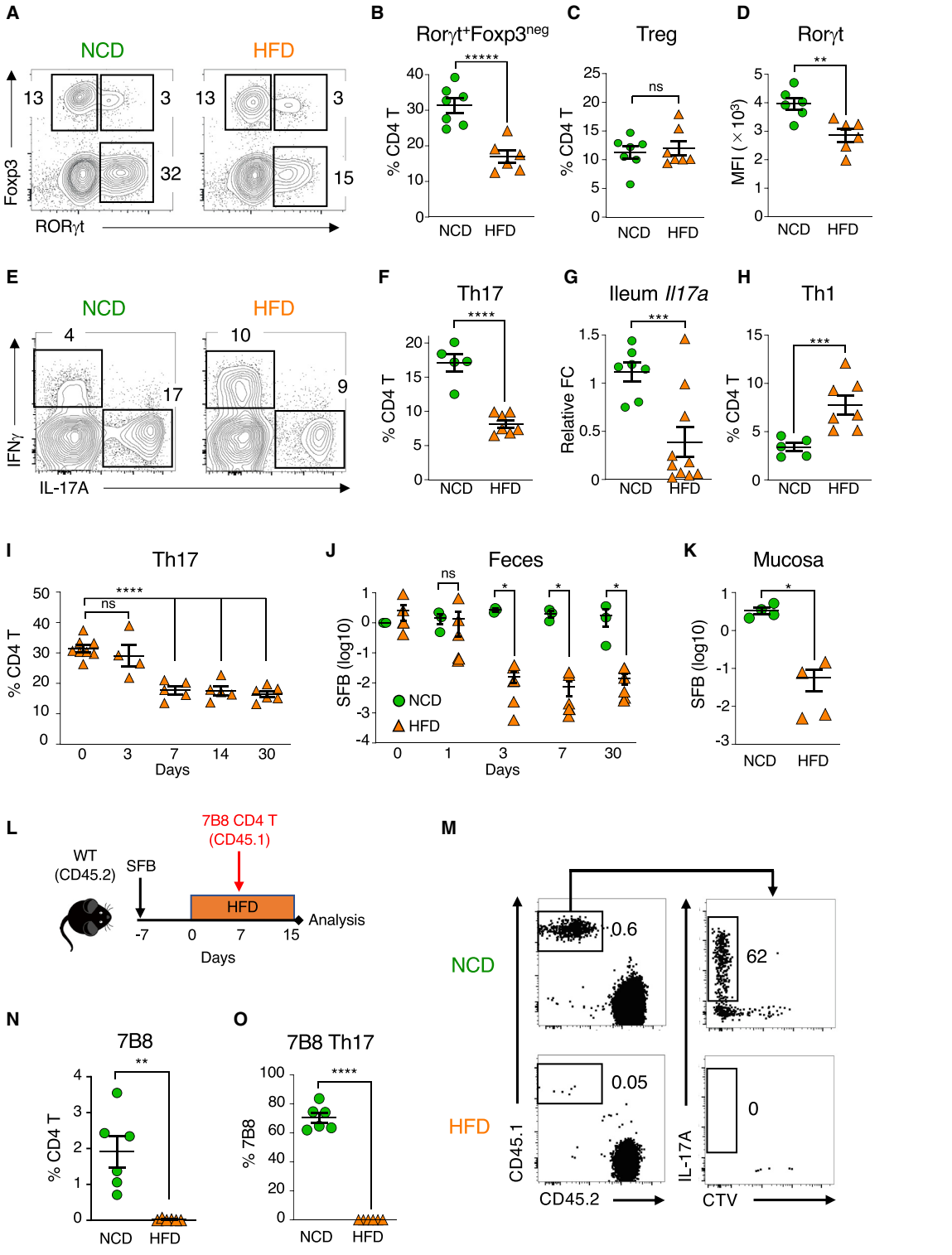

(legend on next page)

metabolic syndrome-associated inflammatory phenotypes (Dalmas et al., 2014; Fabbrini et al., 2013), as well as protection from obesity and metabolic syndrome (Garidou et al., 2015; Hong et al., 2017). Similarly, type 3 innate lymphoid cells (ILC3) and ILC3-derived IL-22 have been reported to exert both protective and promoting effects in metabolic syndrome (Upadhyay et al., 2012; Wang et al., 2014, 2017; Zou et al., 2018). Therefore, the role of type 3 immune cells seems complex and possibly context dependent; however, the nature of the environmental, or other, signals controlling this heterogeneity of function is not known.

Microbiota are important modulators of intestinal immunity, including T cell and ILC3 responses (Honda and Littman, 2016; Ivanov et al., 2022). HFD induces changes in microbiota composition that play crucial role in obesity phenotypes (Ley et al., 2006; Tilg et al., 2020; Turnbaugh et al., 2008). HFD microbiota can promote metabolic syndrome by increasing energy harvest, including calory extraction and intestinal lipid absorption (Petersen et al., 2019; Turnbaugh et al., 2006; Wang et al., 2017), or by inducing intestinal epithelial barrier disruption and endotoxemia, leading to adipose tissue inflammation (Cani et al., 2008). HFD-associated microbiota can also affect metabolic syndrome by modulating immune responses (Tilg et al., 2020). The dietary and microbiota entities that regulate host immunity in the context of metabolic syndrome, as well as the cellular and molecular mechanisms involved, are not known.

Here, we examined the role of microbiota-controlled intestinal immunity, and in particular type 3 immunity, in early induction of DIO and metabolic syndrome. We found that microbiota-induced Th17 cells are protective against DIO and metabolic syndrome. We identified dietary and microbiota components involved, how these components modify Th17 cell-inducing microbiota, and the mechanisms by which they control metabolic syndrome in a context-dependent manner. We also propose an alternative explanation for the pathogenic role of sugar in metabolic disease through suppression of immuno-protective microbiota.

RESULTS

HFD disrupts intestinal immune homeostasis by eliminating Th17-inducing microbiota

To identify initiating events in metabolic syndrome, we examined the effects of HFD on intestinal immune homeostasis at 4 weeks, prior to development of inflammatory changes in adipose tissue (Cani et al., 2008; Kawano et al., 2016). Compared to normal chow diet (NCD), WT mice fed HFD developed metabolic syndrome characteristics, including weight gain, insulin resistance, and glucose intolerance (Figure S1A–S1C). In the small intestinal lamina propria (SI LP), HFD led to a significant decrease in the proportion and total numbers of RORγt^{+}Foxp3^{neg} Th17 cells (Figures 1A, 1B, and S1D) but had no apparent effect on RORγt^{neg} or RORγt^{+} Foxp3^{+} Tregs (Figures 1C and S1E). Moreover, remaining RORγt^{+} Th17 cells had decreased expression of RORγt (Figure 1D), suggesting general loss of Th17 cell functionality. Cytokine staining revealed a corresponding decrease in percentage and total numbers of IL-17^{+} Th17 cells (Figures 1E, 1F, and S1F) and severely reduced tissue levels of *Il17* transcripts in the terminal ileum (Figure 1G) in HFD-fed animals. At the same time, HFD did not affect the levels of other RORγt or IL-17-expressing populations, such as RORγt^{+} γδ T cells or total ILC3 (Figures S1G and S1H). However, HFD feeding was associated with an increase in the proportion of SI LP Th1 cells (Figure 1H), as well as a relative enrichment of CCR6^{+} ILC3 (Figures S1I–S1L), a subset that produces high levels of IL-22 (Klose and Artis, 2016). As expected, at 4 weeks, major inflammatory immune cell subsets in visceral adipose tissue were not significantly changed (Figures S1M and S1N). Therefore, HFD leads to specific decrease in intestinal Th17 cell immunity. The loss of SI LP Th17 cells occurred by day 7 following transition to HFD (Figure 1I) and preceded the increase in inflammatory LP Th1 cells (Figure S1O).

We previously showed that SI LP Th17 cells in specific-pathogen free (SPF) mice are induced by commensal microbiota, particularly segmented filamentous bacteria (SFB) (Goto et al., 2014; Ivanov et al., 2009). Therefore, we investigated whether HFD affects SFB levels. Transition to HFD led to rapid loss of SFB from both feces and ileal mucosa (Figures 1J and 1K). Notably, SFB loss preceded the loss of Th17 cells (Figures 1I and 1J) and occurred in Th17 cell-deficient animals (Figure S1P). Thus, the decrease in SI LP Th17 cells following transition to HFD is secondary to the loss of SFB. To confirm that HFD-induced SFB loss eliminates the induction of SFB-specific Th17 cells, we adoptively transferred congenic SFB-specific 7B8 TCR Tg T cells (Yang et al., 2014) into SFB-positive mice fed NCD or HFD (Figure 1L). 7B8 CD4 T cells expanded and differentiated into Th17 cells in NCD controls (Figures 1M–1O). In contrast, SFB-specific CD4 T cells did not expand or generate Th17 cells

Figure 1. HFD disrupts intestinal immune homeostasis by eliminating Th17-inducing microbiota

(A–F) Flow cytometry for T cell transcription factors (A–D) and cytokines (E and F) in SI LP CD4 T cells in C57BL/6 mice fed NCD or HFD for 4 weeks. Plots gated on TCRβ+CD4^{+} cells. Treg, Foxp3^{+}RORγt^{neg}; Th17, IL-17^{+}IFNγ^{neg}. Data from two out of multiple independent experiments. n = 7 mice/group.

(G) Quantitative RT-PCR of *Il17a* expression in terminal ileum of C57BL/6 mice fed NCD or HFD for 5 weeks. Data combined from three independent experiments. n = 7–10 mice/group.

(H) Th1 cells (IFNγ^{+}IL-17^{neg}) from experiments in (E).

(I and J) Time course of the proportion of Th17 cells (RORγt^{+}Foxp3^{neg}) in SI LP CD4 T cells (I) and SFB levels in feces (J) in C57BL/6 mice fed NCD or HFD. Data from two out of multiple independent experiments n = 3–8 mice/group.

(K) qPCR for SFB 16S DNA in terminal ileum mucosa of C57BL/6 mice fed NCD or HFD for 7 days. Data combined from two independent experiments. n = 4 mice/group

(L) Experimental scheme for (M–O). CD45.2 C57BL/6 mice were colonized with SFB and 7 days later switched to HFD. A week later, the animals received SFB-specific 7B8/CD45.1/IL-17A-GFP TCR Tg CD4 T cells. Tg T cells were analyzed 8 days after transfer.

(M–O) Representative FACS plots (M) and statistics (N and O) of expansion (N) and Th17 cell differentiation (O) of transferred Tg CD4 T cells in SI LP on day 15. Data combined from two independent experiments. n = 6 mice/group.

See also Figure S1.

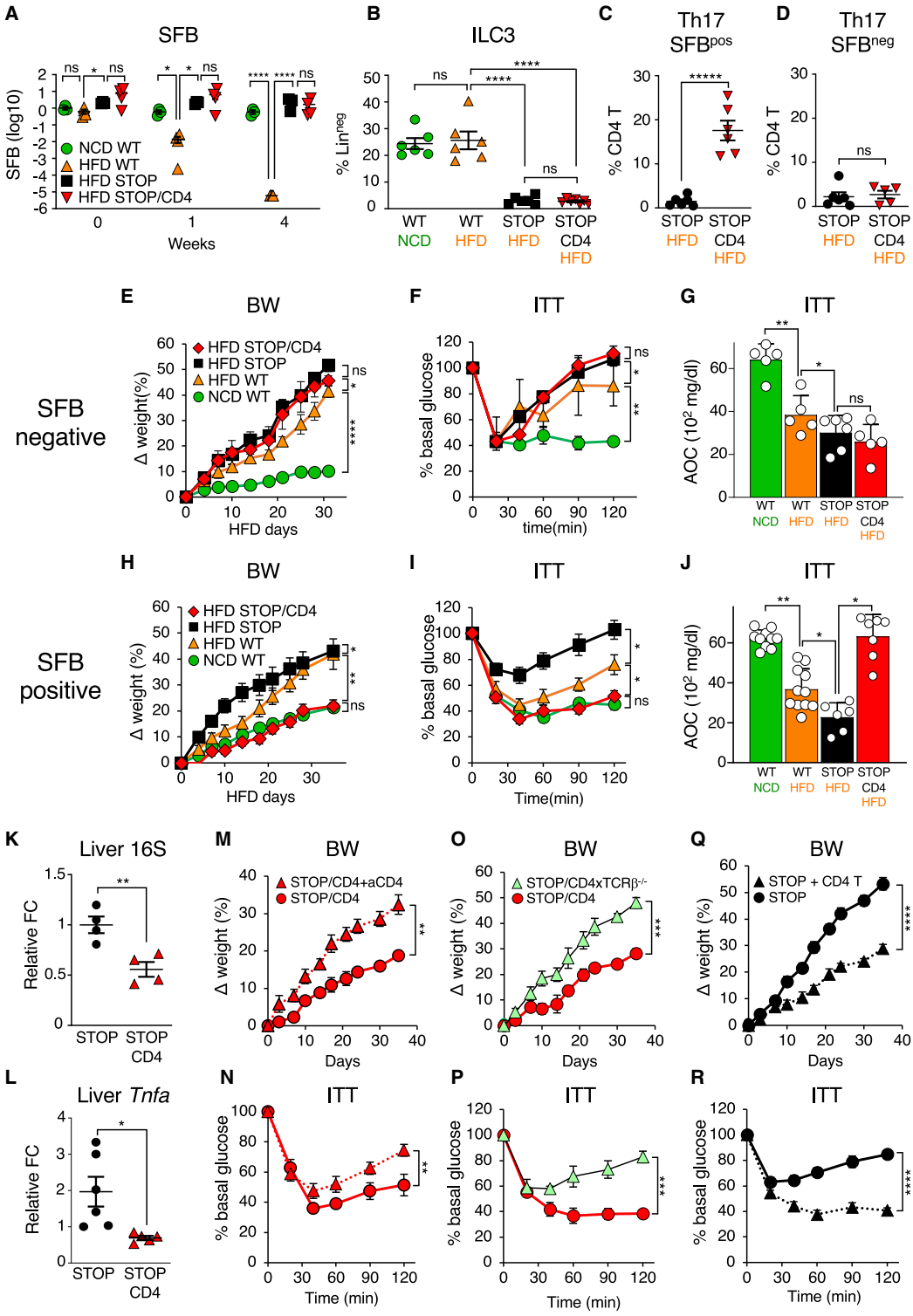

(legend on next page)

in HFD-fed animals (Figures 1M–1O). These results demonstrate that both SFB and SFB-derived T cell antigens are lost following transition to HFD. Collectively, these data suggest that HFD induces rapid loss of Th17 cell-inducing microbiota that leads to loss of homeostatic commensal Th17 cells prior to development of metabolic syndrome.

We also investigated the abundance of previously reported human Th17 cell-inducing bacteria in a published microbiota dataset from non-diabetic adults with or without increased body mass index and metabolic syndrome (Pedersen et al., 2016). A significantly higher proportion of adults with metabolic syndrome showed depletion of community of 20 human Th17-inducing bacteria (Atarashi et al., 2015) (Figure S1Q). Metabolic syndrome adults also had decreased relative abundance of *Bifidobacterium adolescentis* (Tan et al., 2016) but not *Eggerthella lenta* (Alexander et al., 2022) (Figures S1R and S1S). Therefore, metabolic syndrome may also negatively affect Th17-inducing microbiota in humans.

Microbiota-induced Th17 cells protect from metabolic syndrome

Both Th17 cells and ILC3 have been implicated in protection from metabolic syndrome (Garidou et al., 2015; Wang et al., 2014) and are regulated by SFB (Ivanov et al., 2009; Sano et al., 2015). Therefore, we examined the differential role of Th17 cells and ILC3 in metabolic syndrome. Traditionally, this has been difficult to ascertain because all currently available ILC3-depletion models also have perturbed T cell development and/or Th17 differentiation (Klose and Artis, 2016, Tait Wojno and Artis, 2016; Vivier et al., 2018). We generated a genetic model in which ILC3 development is selectively impaired while preserving the T cell compartment (Figure S2). We first generated RORγ-STOP-flox (STOP) mice that lack both ILC3 and Th17 cells (Figure S2A). These animals phenocopy RORγ-knockout (KO) animals (Figures S2B–S2G; data not shown). They have perturbed T cell development in the thymus and do not generate Th17 cells (including SI LP Th17 cells) or ILC3 (Figures S2B–S2G). We crossed STOP mice to T cell-specific CD4-Cre animals to recover RORγ expression in double-positive thymocytes (hence in all T cells). The resulting STOP/CD4-Cre (STOP/CD4) mice recover most αβ T cell development and recover SI LP Th17 cell differentiation but maintain other immune deficiencies present in STOP mice, including the lack of ILC3 (Figures S2B–S2G).

SFB-negative STOP, STOP/CD4, and WT littermate controls were colonized with SFB and fed HFD. After transition to HFD, WT animals quickly lost SFB as before. In contrast, HFD did not lead to loss of SFB in ILC3-deficient mice (STOP or STOP/CD4) (Figures 2A and 2B), suggesting that ILC3 are required for the HFD-mediated loss of SFB. Irrespective of SFB, HFD-fed STOP mice did not generate Th17 cells and had decreased levels of *Il17a* transcripts in the terminal ileum (Figures 2C, 2D, and S3A). In contrast, STOP/CD4 mice colonized with SFB maintained high levels of SI LP Th17 cells even under HFD (Figures 2C and S3A). As expected, SFB-negative STOP/CD4 mice lacked SI LP Th17 cells (Figure 2D).

Next, we compared the development of DIO and metabolic syndrome in ILC3/Th17-deficient STOP mice and ILC3-deficient/Th17-sufficient STOP/CD4 mice. In the absence of SFB-induced Th17 cells (Figure 2D), both strains of ILC3-deficient mice demonstrated weight gain (Figure 2E) and metabolic syndrome phenotypes, i.e., increased insulin resistance and glucose intolerance (Figures 2F, 2G and S3B). Moreover, weight gain and metabolic syndrome phenotypes in ILC3-deficient STOP and SFB-negative STOP/CD4 mice were slightly, but significantly, increased compared to WT controls (Figures 2E–2J, S3B, and S3C). In the presence of SFB Th17 cells (Figure 2C), STOP/CD4 mice resembled NCD-fed WT controls and were protected from DIO, including weight gain (Figure 2H) and increased adiposity (Figures S3D and S3E), as well as from pre-diabetic phenotypes associated with metabolic syndrome (Figures 2I,2J, and S3C). Protection was not mediated by changes in brown fat adiposity or food intake (Figures S3F and S3G). In addition to maintaining SI LP Th17 cells (Figure 2C), HFD-fed SFB-positive STOP/CD4 mice had significantly decreased levels of transcripts for the Th1 cytokine IFNγ in the SI LP compared to HFD-fed WT or STOP mice (Figure S3H). They also demonstrated decreased liver pathology, including decreased bacterial translocation and expression of *Tnfa* transcripts (Figures 2K and 2L). The protection from metabolic syndrome in SFB-positive STOP/CD4 mice was also evident at 8 weeks (Figures S3I and S3J). Therefore, protection from DIO

Figure 2. Microbiota-induced Th17 cells protect from metabolic syndrome

(A) qPCR for SFB 16S DNA in feces from WT, STOP, and STOP/CD4 mice fed NCD or HFD for indicated times. Data from two out of several independent experiments. n = 3–5 mice/group.

(B) ILC3 in SI LP of WT, STOP, and STOP/CD4 mice fed NCD or HFD for 5 weeks. Data from two out of multiple independent experiments. n = 5–6 mice/group.

(C and D) SI LP Th17 cells (IL-17A^{+}IFNγ^{neg}) in SFB-positive (C) and SFB-negative (D) STOP and STOP/CD4 mice on day 40 of HFD feeding. Data from three (C) or two (D) independent experiments out of multiple experiments. n = 6–7 mice/group.

(E–J) Metabolic analysis of SFB-negative (E–G) and SFB-positive (H–J) mice of the indicated genotypes fed NCD or HFD for 4–5 weeks. SFB-positive mice were colonized with SFB by oral gavage 2 weeks prior to diet transition. (E and H) Changes in body weight. (F, G, I, and J) Insulin tolerance test on day 28 of HFD. AOC, area over the curve. Data from two (E–G) or three (H–J) independent experiments out of several experiments. n = 6–11 mice/group.

(K and L) qPCR for total bacterial 16S DNA (K) and quantitative RT-PCR for *Tnfa* transcripts in the liver of STOP and STOP/CD4 mice fed HFD for 5 weeks. Data combined from two independent experiments. n = 4–6 mice/group.

(M and N) Body weight change (M) and insulin tolerance test at day 28 (N) of SFB-positive STOP/CD4 mice treated with IgG control or anti-CD4 neutralizing antibody and fed HFD for 5 weeks. Data combined from two independent experiments. n = 5 mice/group.

(O and P) Body weight change (O) and insulin tolerance test at day 28 (P) of HFD-fed SFB-positive STOP/CD4 and T cell-deficient STOP/CD4 mice (TCRβ$^{-/-}$/RORγ-STOP/CD4-Cre). Data combined from two independent experiments. n = 7 mice/group.

(Q and R) Body weight change (Q) and insulin tolerance test at day 28 (R) of HFD-fed SFB positive STOP mice with and without transfer of total WT CD4 T cells. Data combined from two independent experiments. n = 5 mice/group.

See also Figures S2 and S3.

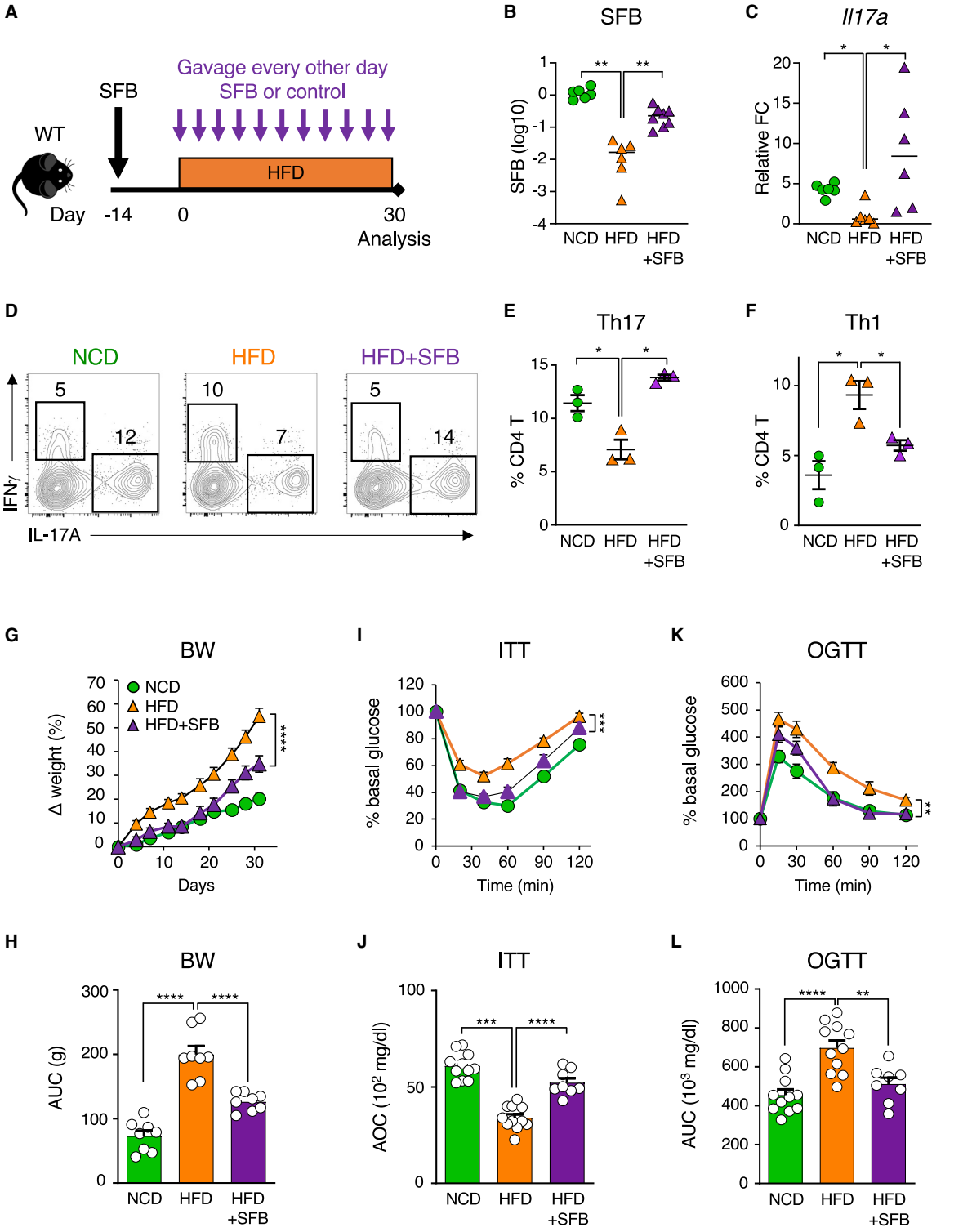

(legend on next page)

and metabolic syndrome in STOP/CD4 mice correlates with the presence of SFB-induced Th17 cells.

To confirm that protection is mediated by CD4 T cells, we depleted CD4 T cells in SFB/Th17-positive STOP/CD4 mice using anti-CD4 antibody (Figure S3K) and administered a HFD. Depletion of CD4 T cells did not affect SFB levels in HFD-fed STOP/CD4 mice (Figure S3L). However, protection from DIO and metabolic syndrome was lost in CD4 T cell-depleted STOP/CD4 mice (Figures 2M, 2N, and S3M). We also crossed STOP/CD4 mice to TCRβ-KO animals to genetically delete αβ T cells. TCRβKO-STOP/CD4 animals became susceptible to DIO and metabolic syndrome (Figures 2O, 2P, and S3N), despite maintenance of SFB (Figure S3O). Together, these experiments demonstrate that commensal Th17 cells are required for microbiota-mediated protection against DIO and metabolic syndrome.

To investigate whether Th17 cells are sufficient to bestow protection, we transferred WT CD4 T cells into SFB-colonized metabolic syndrome-susceptible STOP mice (Figure S3P). Transfer of CD4 T cells did not affect SFB levels (Figure S3Q). Transferred WT CD4 T cells differentiated into Th17 cells locally in the SI LP (Figure S3R; Goto et al., 2014; Sano et al., 2015). STOP mice adoptively transferred with CD4 T cells were significantly protected from DIO and metabolic syndrome compared to untreated animals (Figures 2Q and 2R). The foregoing studies suggest that gut microbiota can mediate protection from metabolic syndrome through induction of intestinal Th17 cells. Microbiota-induced Th17 cells appear to be both necessary and sufficient to provide protection and prevent or suppress development of obesity and pre-diabetic phenotypes.

Probiotic Th17 cell-inducing bacteria ameliorate metabolic syndrome

Our results demonstrated that one of the pathogenic effects of HFD is the depletion of homeostatic commensal intestinal Th17 cells through elimination of Th17 cell-inducing microbiota. We hypothesized that recovery of intestinal Th17 cells by maintaining Th17 cell-inducing microbiota under HFD can improve DIO and metabolic disease. Therefore, we treated SFB-positive HFD-fed WT mice with SFB or control bacteria by oral gavage every other day for 4 weeks (Figure 3A). HFD-fed animals gavaged with control bacteria lost SFB (Figure 3B), which led to a decrease of intestinal *Il17a* transcripts (Figure 3C), due to a decrease of SI LP Th17 cells (Figures 3D and 3E). The animals also developed obesity and metabolic disease (Figures 3G–3L). SFB administration led to partial, but significant, recovery of SFB levels in fecal contents (Figure 3B). Importantly, SFB-treated animals had significant recovery of SI LP Th17 cells (Figures 3D and 3E) and IL-17 expression in terminal ileum (Figure 3C). Compared to controls, SFB-treated animals had significantly reduced weight gain under HFD (Figures 3G and 3H) and were protected from development of pre-diabetic phenotypes, including insulin resistance (Figures 3I and 3J) and glucose intolerance (Figures 3K and 3L). SFB-treated animals also showed amelioration of HFD-induced intestinal inflammation, including a decrease in inflammatory Th1 cells (Figure 3F), transcripts for inflammatory T cell cytokines, e.g., IFN-γ and TNF-α (Figures S4A and S4B), and transcripts for markers of tissue inflammation (Figures S4C and S4D). We conclude that a probiotic regimen of Th17 cell-inducing microbiota can significantly ameliorate DIO and metabolic syndrome by recalibrating intestinal T cell homeostasis.

Dietary sugar promotes metabolic syndrome through elimination of commensal Th17 cells

Next, we investigated the nature of the dietary components that lead to loss of protective commensal intestinal Th17 cells. We used loss of SFB as a readout to identify dietary ingredients that deplete intestinal Th17 cells. Two of the better-characterized deleterious nutritional components of HFD are excess fat and low dietary fiber. However, neither removal of excess fat from our HFD formulation by using control purified low-fat diet (LFD) nor the addition of dietary fiber in the form of inulin improved SFB maintenance (Figure 4A). In contrast to less well-defined grain-based NCD, HFD is a purified diet that contains defined ingredients. Therefore, numerous nutritional components differ between the two formulations. We asked whether the loss of SFB is due to presence of an inhibitory activity or lack of a nutritional component in HFD, as compared to NCD. To answer this question, we provided mice with both diets simultaneously. We reasoned that if HFD contains an excess of an inhibitory component, then it should still inhibit SFB even in the presence of NCD. Alternatively, a missing nutritional component will be recovered by complementation with NCD. WT mice were colonized with SFB and then fed NCD, HFD, or a 50:50 mix of the two diets (Figure 4B). The addition of NCD nutritional components as a 50:50 NCD:HFD mix did not prevent SFB decrease (Figure 4B). This suggested that HFD contains an "inhibitory" component, prompting us to focus on the ingredients enriched in the HFD formulation. In addition to dietary fat, another ingredient highly represented in HFD is dietary sugar. Whereas NCD formulations contain 3%–6% sugar, HFD formulations contain 25% dietary sugars, including 10% sucrose and 15% maltodextrin. Sucrose and maltodextrin (a common ingredient in packaged foods, including candies and soft drinks) are thought to increase risk of metabolic syndrome, although the mechanisms

Figure 3. Probiotic Th17 cell-inducing bacteria ameliorate metabolic syndrome

(A) Experimental scheme of probiotic treatment.

(B) qPCR for SFB 16S DNA in feces on day 28 of HFD. n = 6–8 mice/group.

(C) Quantitative RT-PCR of *Il17a* transcripts in terminal ileum at 5 weeks on HFD. n = 6 mice/group.

(D–F) Flow cytometry of cytokines in SI LP CD4 T cells at 5 weeks on HFD. n = 3 mice/group.

(G–L) Metabolic analysis, including body weight change (G and H), insulin tolerance test (I and J), and oral glucose tolerance test (K and L) at 4 weeks. n = 8–11 mice/group.

Data combined from two independent experiments with similar results. AOC, area over the curve; AUC, area under the curve.

See also Figure S4.

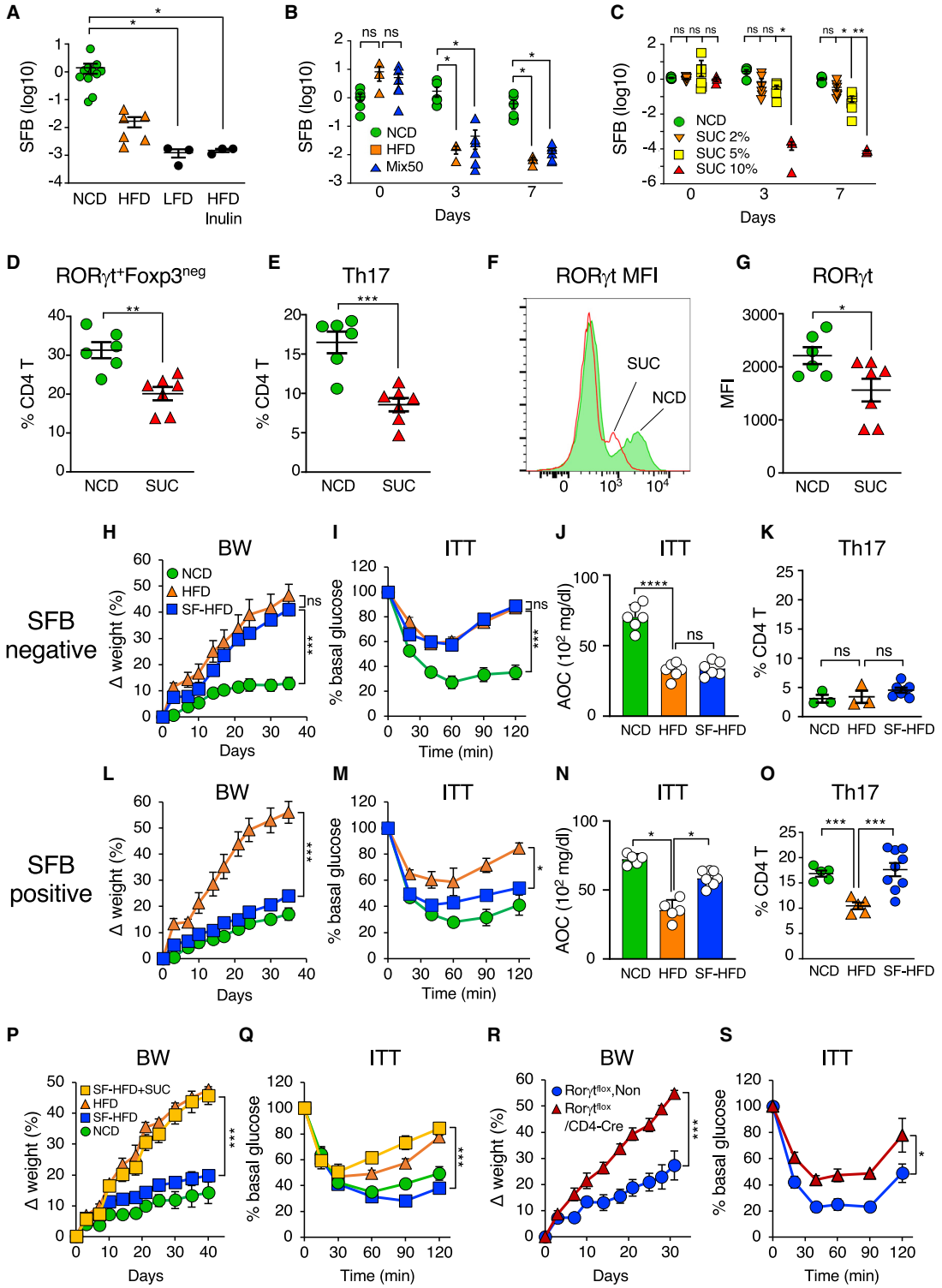

(legend on next page)

remain controversial (Bravo et al., 2013; Johnson et al., 2013; Macdonald, 2016; Malik et al., 2010). Sugar levels in diet formulations inversely correlated with the diets' effects on SFB levels (Figure S5A). Sucrose, provided *ad libitum* into the drinking water of NCD-fed WT animals, eliminated SFB in a dose-dependent manner (Figure 4C). 10% w/v sucrose or maltodextrin decreased SFB levels in feces and ileal mucosa of NCD-fed mice with similar kinetics to HFD-fed animals (Figures 4C, S5B, and S5C). In contrast, 10% galactose did not significantly affect SFB levels (Figure S5C). Next, we examined the effects of sucrose on intestinal Th17 cells. Addition of sucrose to the water of NCD-fed animals decreased both RORγt^{+} and IL-17^{+} Th17 cells in SI LP (Figures 4D and 4E), similarly to HFD (compare to Figure 1). As observed with HFD, the remaining Th17 cells in sucrose-fed animals had decreased levels of RORγ, suggesting perturbed functionality (Figures 4F and 4G). Other intestinal CD4 T cell subsets were not significantly affected by sucrose (Figure S5D–S5F). Examination of a published human personalized diet-microbiome dataset (Johnson et al., 2019) revealed that increased sugar consumption was associated with decrease in the relative abundance of Th17 cell-inducing microbes in human volunteers (Figure S5G).

To investigate the role of dietary sugar on Th17 cell-mediated protection, we generated sugar-free HFD (SF-HFD) by replacing sucrose and maltodextrin in the HFD with starch. SF-HFD induced obesity and metabolic syndrome similarly to control HFD in SFB-negative animals (Figures 4H–4K and S5H). In contrast, SFB-colonized SF-HFD-fed mice were protected from weight gain (Figure 4L), insulin resistance (Figures 4M and 4N), and glucose intolerance (Figure S5H). In contrast to HFD-fed mice, SFB-gavaged SF-HFD-fed animals maintained high levels of protective intestinal Th17 cells (Figures 4O). SFB-gavaged SF-HFD-fed animals also lacked evidence of intestinal and systemic inflammation and had low levels of inflammatory Th1 cells in SI LP (Figure S5I) and decreased levels of bacterial DNA and *Tnfa* transcripts in the liver (Figures S5J and S5K). Protection was also present at 9 weeks (Figures S5L and S5M).

To confirm that the positive effects of SF-HFD are due to absence of sugar and to control for other potential diet effects, we performed a separate set of experiments in which some SF-HFD animals received 10% sucrose in the drinking water. As before, SFB-colonized SF-HFD-fed animals maintained intestinal Th17 cells and were protected from DIO and metabolic syndrome (Figures 4P and 4Q). The protection afforded SF-HFD-fed mice, however, was entirely lost when sugar was added to their drinking water. The animals lost intestinal Th17 cells and were as susceptible as HFD-fed animals to obesity and metabolic syndrome (Figures 4P, 4Q, S5N, and S5O).

To confirm that the protective effects of SF-HFD are mediated by Th17 cells, we examined RORγt-flox/CD4-Cre animals that specifically lack Th17 cell differentiation (Choi et al., 2016). RORγt-flox/CD4-Cre and control littermates were colonized with SFB and fed SF-HFD. As expected, RORγt-flox/CD4-Cre animals lacked intestinal Th17 cells (Figure S5P). At the same time, protection from DIO and metabolic syndrome was lost in these animals compared with control WT littermates (Figures 4R and 4S). Compared to WT littermates, Th17 cell-deficient mice on SF-HFD showed increased weight gain (Figure 4R), insulin resistance (Figure 4S), glucose intolerance (Figure S5Q), and increased bacterial translocation and inflammatory markers in the liver (Figure S5R and S5S). Collectively, the foregoing data suggest that dietary sugar counteracts the protective effects of intestinal commensal Th17 cells in the context of DIO and metabolic syndrome by depleting these cells. They also show that elimination of dietary sugar is not sufficient to provide therapeutic benefit; protection also requires presence of commensal Th17 cells. Therefore, dietary interventions may need to be combined with immune therapies to achieve desired effects.

Dietary sugar displaces Th17 microbiota by increasing a member of *Erysipelotrichiaceae*

We next investigated the mechanism by which dietary sugar displaces SFB and metabolic syndrome-protective Th17 cells. Similarly to HFD, sugar did not decrease SFB in ILC3-deficient mice (Figure S6A), suggesting that sugar does not directly affect these Th17-inducing bacteria. To account for host effects, we treated SFB-monocolonized WT animals with 10% sucrose in the drinking water. In contrast to SPF mice (Figure 4C), dietary sugar did not affect SFB levels in monocolonized mice (Figure 5A). Therefore, displacement of SFB by sugar requires the presence of commensal microbes. To identify commensal species that mediate the effects of sugar, we compared microbiota

Figure 4. Dietary sugar promotes metabolic syndrome through elimination of commensal Th17 cells

(A) SFB 16S DNA in feces from C57BL/6 mice fed natural ingredients normal chow diet (NCD) and various purified diets for 1 week. LFD, low-fat diet; HFD Inulin, HFD supplemented with inulin. Data combined from two independent experiments. n = 3–11 mice/group.

(B) SFB 16S DNA in feces from C57BL/6 mice fed NCD, HFD, or a 50:50 mix NCD:HFD. Data combined from two independent experiments. n = 3–6 mice/group.

(C) SFB 16S DNA in feces from C57BL/6 mice fed NCD plus various concentrations of sucrose (SUC) in the drinking water. Data from two out of multiple independent experiments. n = 3–7 mice/group.

(D–G) RORγt+ (D) Th17 cells, IL-17A+ (E) Th17 cells, and RORγt expression in Foxp3^{neg}TCRβ^{+}CD4^{+} cells (F and G) in SI LP of mice fed NCD with and without 10% SUC in the drinking water for 1 week. Data from two out of multiple independent experiments. n = 6–7 mice/group.

(H–O) Metabolic and immune cell phenotypes of SFB-negative (H–K) or SFB-gavaged (L–O) C57BL/6 mice fed NCD, HFD, or sugar-free HFD (SF-HFD) for 4 weeks. SFB-gavaged mice were colonized with SFB by oral gavage 2 weeks prior to the change of diet. (H and L) changes in body weight. (I, J, M, and N) insulin tolerance test on day 28. (K and O) SI LP Th17 cells (IL-17A^{+}IFNγ^{neg}) as proportion of TCRβ^{+}CD4^{+} cells on day 40. Data from two out of four independent experiments. n = 5–9 mice/group.

(P and Q) Body weight change (P) and insulin tolerance test on day 28 (Q), of SFB-colonized C57BL/6 mice fed NCD, HFD, SF-HFD, or SF-HFD supplemented with 10% sucrose (SUC) in the drinking water for 5 weeks. Data combined from two independent experiments. n = 5 mice/group.

(R and S) Body weight change (R) and insulin tolerance test on day 28 (S), of SFB-colonized Th17 cell-deficient RORγt$^{flox/flox}$/CD4-Cre mice and control littermates fed SF-HFD. Data combined from two independent experiments. n = 5 mice/group.

See also Figure S5.

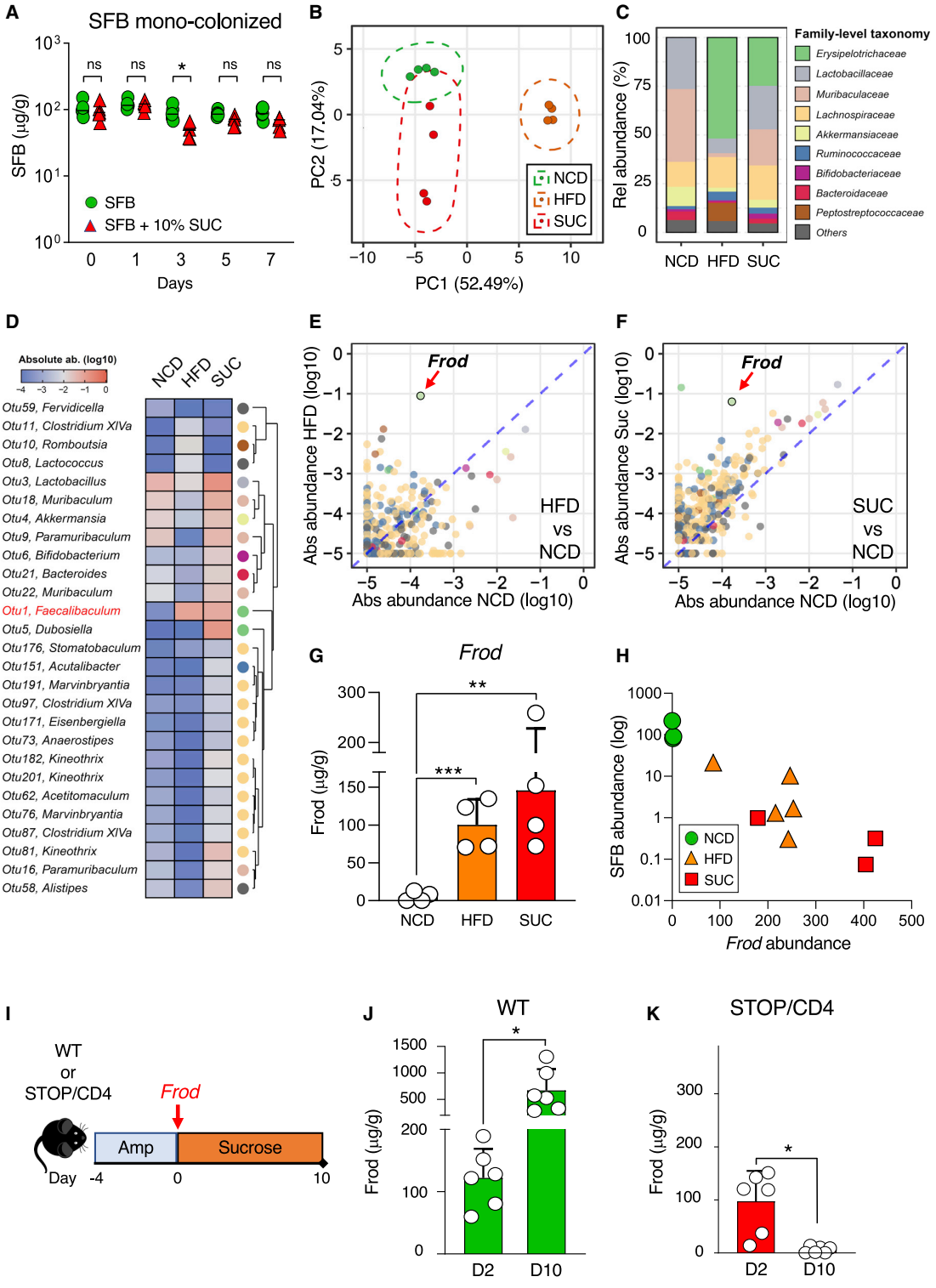

(legend on next page)

composition of animals fed NCD, HFD, or NCD + 10% sucrose in the drinking water (Figures 5B–5F). HFD-fed and sugar-treated animals had distinct microbiota composition from that of NCD-fed animals but also significantly differed from each other (Figure 5B). This allowed us to narrow down microbiota differences between Th17-depleting (HFD and sugar) and Th17-supporting (NCD) diets. At the family level, *Erysipelotrichaceae*, *Ruminococcaceae*, and *Lachnospiraceae* were upregulated in both Th17-depleting diets (Figure 5C). *Erysipelotrichaceae* was by far the highest and most significantly enriched family in both HFD and sugar over the NCD (Figure 5C). Erysipelotrichaceae expansion has been reported in metabolic disorders, including DIO in mice (Turnbaugh et al., 2008), as well as in obese humans (Zhang et al., 2009). *Erysipelotrichaceae* expansion in our dataset contained several operational taxonomic units (OTU). However, one particular OTU, identified as *Faecalibaculum rodentium* (*Frod*), was consistently overrepresented in both HFD and sugar-treated animals (Figures 5D–5F). We confirmed expansion of *Frod* in HFD and sugar-treated mice by qPCR (Figure 5G). Comparison of SFB and *Frod* levels in individual animals identified strong inverse correlation between the two microbiota members (Figure 5H). Sugar-mediated *Frod* expansion was dose-dependent (Figure S6B) and was also present in other dietary treatments that eliminated SFB (Figure S6C) but not in dietary treatments that maintained SFB (Figure S6D). HFD-mediated expansion of *Frod* did not require SFB (Figure S6E). Moreover, it preceded the loss of SFB in SFB-positive animals (Figure S6F). We therefore hypothesized that *Frod* expansion may be responsible for the loss of SFB in SPF mice. In agreement with this hypothesis, neither sugar nor HFD increased *Frod* in ILC3-deficient mice, which maintain SFB (Figure S6G; data not shown). To investigate whether this is because of inability of *Frod* to colonize or expand in ILC3-deficient mice, we compared colonization kinetics following dietary intervention. For this, we first eliminated endogenous *Frod* by pre-treating WT and ILC3-deficient STOP/CD4 mice with ampicillin (Amp). We next introduced exogenous *Frod* by oral gavage and followed colonization kinetics. To examine *Frod,* expansion animals were also given 10% sucrose in the drinking water (Figure 5I). Shortly after *Frod* gavage (day 2), both WT and STOP/CD4 mice showed similarly high levels of *Frod* in feces (Figures 5J and 5K), suggesting that *Frod* is capable of colonizing ILC3-deficient animals. Sugar in the drinking water led to a robust expansion of *Frod* in WT mice by day 10 (Figure 5J). In contrast, *Frod* was almost undetectable at day 10 in sugar-treated STOP/CD4 mice (Figure 5K). The foregoing results demonstrate that sugar-mediated expansion of *Frod* requires ILC3.

The above results strongly suggest that sugar or HFD-mediated expansion of *Frod* is responsible for the loss of SFB. Therefore, we used gnotobiotic animals to directly test whether *Frod* is sufficient to outcompete or displace SFB. We first attempted to colonize germ-free (GF) mice with SFB and *Frod* by gavaging both bacteria at the same time (Figure 6A). SFB colonized GF animals to high levels when provided alone (Figure 6B). In contrast, SFB levels were 100-fold lower when SFB and *Frod* were gavaged together (Figures 6B and 6C). Addition of sugar to the drinking water of SFB/*Frod* dually colonized animals led to expansion of *Frod* and even further decrease in SFB levels (Figures 6D–6F). We also asked whether *Frod* can displace pre-existing SFB. GF animals were first colonized with SFB and later colonized with *Frod* or control bacteria (Figures 6G and S6H). All animals were similarly colonized with SFB prior to the introduction of *Frod* (Figures 6H and S6I). However, SFB quickly disappeared after introduction of *Frod* (Figures 6H and 6I) but not after introduction of control bacteria (Figure S6I–S6K). In accordance with the loss of SFB, *Frod* colonization was also accompanied by a decrease of SFB-induced intestinal Th17 cells (Figures S6L–S6O). 24 h after *Frod* gavage, SFB and *Frod* were present together in gnotobiotic animals and occupied the same geographical niche in the mucus of terminal ileum close to epithelial cells and also in close proximity to each other (Figures 6J and 6K). These findings suggest that dietary sugar expands members of the *Erysipelotrichaceae* family, and specifically *Frod*, in an ILC3-dependent manner, which in turn can displace SFB and decrease protective intestinal Th17 cells.

Commensal Th17 cells protect from metabolic syndrome by regulating intestinal lipid absorption

We next investigated the mechanism by which commensal Th17 cells provide protection from metabolic syndrome. IL-17 has strong effects on intestinal epithelial cells (IECs) and maintains barrier integrity (Hueber et al., 2012; Lee et al., 2015; O'Connor et al., 2009). In the gut, epithelial absorption of dietary lipids is a known regulator of metabolic syndrome (Petersen et al., 2019; Wang et al., 2017). We therefore examined the effects of commensal Th17 cells on intestinal lipid absorption. We compared lipid concentrations in various tissues in HFD-fed Th17-deficient STOP mice that develop metabolic syndrome

Figure 5. Dietary sugar displaces Th17 microbiota by increasing *Faecalibaculum rodentium*

(A) SFB 16S DNA in feces of germ-free mice monocolonized with SFB and fed NCD or NCD plus 10% sucrose (SUC) in the drinking water. Data from one out of two independent experiments. n= 5 mice/group.

(B) PCoA plot of 16S microbiota analysis in feces from WT mice on NCD, 10 days on HFD, or 10 days on NCD plus 10% sucrose in drinking water. Data from one out of two independent experiments. n = 4 mice/group.

(C and D) Family level taxonomy and relative abundance (C) and OTU taxonomy and absolute abundance (D) in 16S analysis of microbiota in the groups in (B).

(E and F) Enrichment analysis of absolute abundance of microbiota OTUs comparing (E) HFD versus NCD and (F) NCD+10% sucrose versus NCD.

(G) qPCR data for *Faecalibaculum rodentium* (*Frod*) in feces from WT mice on NCD, or10 days on HFD, or 10 days on NCD plus 10% sucrose in drinking water. Data from one out of two independent experiments. n = 4 mice/group.

(H) Correlation of SFB and *Frod* levels in individual animals. Data from one out of two independent experiments. n = 3–5 mice/group.

(I–K) Sugar-mediated *Frod* expansion requires ILC3. (I) Experimental scheme. WT and STOP/CD4 mice were pre-treated with Ampicillin (Amp) before introducing *Frod* by oral gavage and 10% sucrose in the drinking water. *Frod* levels in feces of (J) WT or (K) ILC3-deficient STOP/CD4 mice on day 2 (D2) and day 10 (D10) post gavage. Data combined from two independent experiments. n = 6 mice/group.

See also Figure S6.

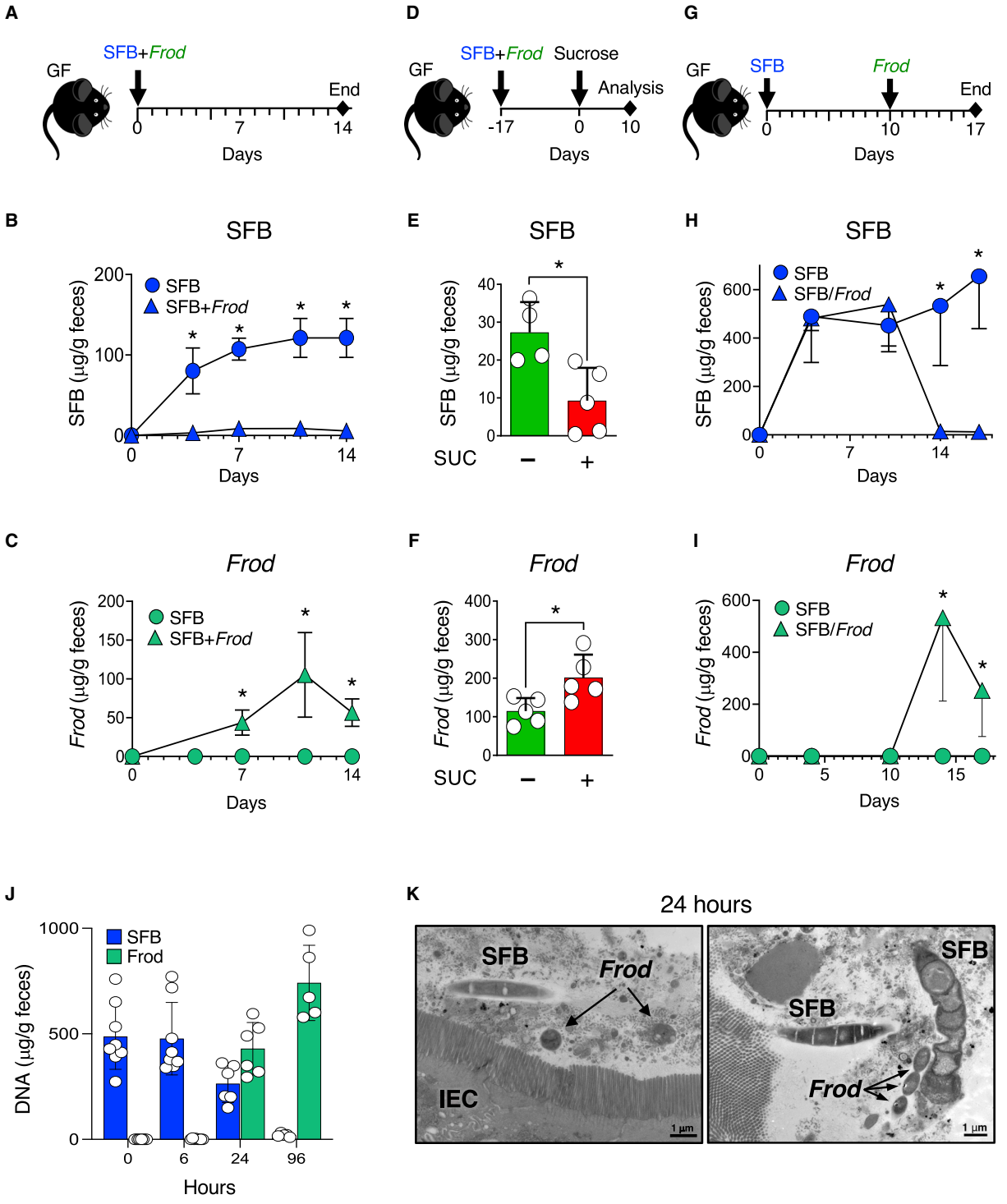

Figure 6. *Faecalibaculum rodentium* is sufficient to displace SFB

(A–C) Germ-free C57BL/6 mice were colonized with SFB, either alone or together with *Frod*. (A) Experimental scheme. (B) SFB and (C) *Frod* levels were followed in feces for 2 weeks. Data from one out of two independent experiments. n = 5 mice/group.

(legend continued on next page)

and Th17-sufficient STOP/CD4 mice in which Th17 cells protect from metabolic syndrome. STOP/CD4 mice had significantly decreased lipid content in IECs and liver (Figures 7A and 7B) but increased lipid levels in feces (Figure 7C). This suggested that lipid absorption in IEC is reduced in the presence of Th17 cells, with concomitant accumulation of lipid in the gut lumen. Indeed, expression of several genes involved in lipid uptake and transport were downregulated in IEC of STOP/CD4 mice (Figures 7D and S7A–S7D), most notably *Cd36*, encoding a transporter of dietary fatty acids into cells (Silverstein and Febbraio, 2009) (Figures 7D and S7E). Downregulation of CD36 in STOP/CD4 IEC required T cells insofar as it was not observed in IEC from HFD-fed αβ T cell-deficient STOP/CD4 mice (Figure 7E). Moreover, CD36 downregulation was not mediated by IL-22 because both strains lack ILC3, and we did not detect a difference in IL-22 production from CD4 T cells (Figure S7F) or in expression of IL-22 controlled genes in intestinal epithelium (Figure S7G; data not shown).

Epithelial CD36 has potent effects on dietary lipid absorption, thereby regulating metabolic syndrome (Nauli et al., 2006; Petersen et al., 2019; Wang et al., 2017). CD36 is highly expressed in the duodenum, where lipid breakdown occurs, as well as the jejunum, where most lipid absorption occurs, and its expression is lower in ileum at steady state (Chen et al., 2001) (Figure 7F–7H). We found that SFB colonization specifically downregulates CD36 gene expression in the distal SI (jejunum and ileum) but not in the duodenum (Figure 7F–7H). CD36 downregulation was dependent on Th17 cell-derived IL-17 because it was not observed in Th17-deficient RORγt-flox/CD4-Cre mice (Figures 7F–7H), IL-17A-deficient mice (Figures 7I and S7H–S7J), or WT animals treated with neutralizing anti-IL-17A antibody (Figure 7J). Thus, commensal Th17 cells can decrease lipid absorption in distal SI by decreasing lipid uptake through CD36 in an IL-17-dependent manner. To investigate whether IL-17 acts directly on the IEC, we examined the effects of IL-17 on CD36 expression in SI enteroids in data from two independent published datasets. Analysis of bulk RNA sequencing (RNA-seq) data from (Kumar et al., 2016) revealed significant decrease of CD36 expression in terminal ileum enteroids treated with IL-17 *in vitro* (Figure 7K). Analysis of single-cell RNA-seq data from total SI enteroids from Biton et al. (2018) showed a similar decrease of CD36 in SI enterocytes treated with IL-17 *in vitro* (Figures S7K and S7L), although the difference did not reach statistical significance. Together, these data suggest that Th17 cell-derived IL-17 can directly suppress CD36 expression in SI enterocytes.

At steady state, lipid absorption predominantly occurs in the jejunum; however, during DIO and in HFD-fed animals, excess lipids carry over into the distal gut (Figure S7M) and are taken up in the ileum (Buttet et al., 2016; de Wit et al., 2012). We found that HFD specifically and potently upregulates CD36 expression in the terminal ileum (and to lesser extent in the jejunum) (Figure S7N). We hypothesized that sugar-sensitive commensal Th17 cells can protect by counteracting the upregulation of CD36. Indeed, both HFD and SF-HFD induced similar upregulation of CD36 in the ileum and jejunum IEC in absence of SFB-specific Th17 cells (Figure 7L). However, this upregulation was significantly suppressed in the presence of commensal Th17 cells in SF-HFD-fed animals (Figures 7L and S7O).

To directly address whether the protective effects of Th17 cells require CD36, we fed SFB-negative and SFB-colonized WT and CD36-deficient animals SF-HFD. As earlier, SFB-induced Th17 cells provided protection from SF-HFD-induced metabolic syndrome in WT animals (Figure 7M–7Q). CD36-deficient animals developed significantly less metabolic syndrome compared to WT animals, as previously reported (Figures 7M–7Q). However, in contrast to WT animals, SFB Th17 cells did not provide additional protection in the absence of CD36 (Figures 7M–7Q). The foregoing findings suggest that commensal Th17 cell-derived IL-17 decreases lipid uptake and absorption specifically in the distal SI during DIO by controlling epithelial expression of the fatty acid transporter CD36.

DISCUSSION

Microbiota and intestinal immunity regulate obesity and metabolic syndrome. Inflammatory changes in the intestine precede liver and adipose tissue inflammation, which drive pathology in metabolic diseases such as metabolic syndrome and T2D (Tilg et al., 2020; Winer et al., 2016). Imbalance of intestinal immune homeostasis is an important initial step in the pathogenesis of these systemic conditions (Kawano et al., 2016; Luck et al., 2015). Here we provide evidence that microbiota-regulated intestinal immunity can also provide protection and should therefore be considered critical therapeutic target in metabolic syndrome and T2D.

The role of type 3 immunity in DIO and metabolic syndrome is complex. Pro-inflammatory Th17 cells are enriched in liver and adipose tissue of obese patients (Dalmas et al., 2014; Fabbrini et al., 2013). At the same time, intestinal Th17 cells have been proposed to provide protection (Garidou et al., 2015; Hong et al., 2017; Perez et al., 2019). Similarly, ILC3 and ILC3-derived IL-22 are considered guardians of the epithelial barrier and beneficial in metabolic syndrome (Wang et al., 2014; Zou et al., 2018). However, ILC3-derived IL-22 can also contribute to metabolic disease (Sasaki et al., 2019; Upadhyay et al., 2012; Wang et al., 2017). Our results help reconcile these seemingly contradicting reports and suggest that the role of ILC3 is context dependent. Using an ILC3-deficient model that allows for differentiation of Th17 cells, we find that ILC3 provide protection from metabolic disease in the absence of SFB and SFB Th17 cells.

(D–F) Germ-free C57BL/6 mice were colonized with SFB and *Frod* for 17 days before addition of 10% sucrose (SUC) in the drinking water. (D) Experimental scheme. (E) SFB and (F) *Frod* levels in feces 10 days after SUC introduction. n = 4 mice/group.
(G–I) Germ-free C57BL/6 mice were colonized with SFB and 10 days later colonized with *Frod*. (G) Experimental scheme. (H) SFB and (I) *Frod* levels were followed in feces for 17 days. Data from two out of four independent experiments. n = 7–8 mice/group.
(J) SFB-monocolonized mice were gavaged with *Frod* and bacteria levels were followed in feces. n = 6–8 mice/group.
(K) Transmission electron microscopy of terminal ileum at the 24-h timepoint of (J). SFB and *Frod* in the mucus (left) and lumen (right).
See also Figure S6.

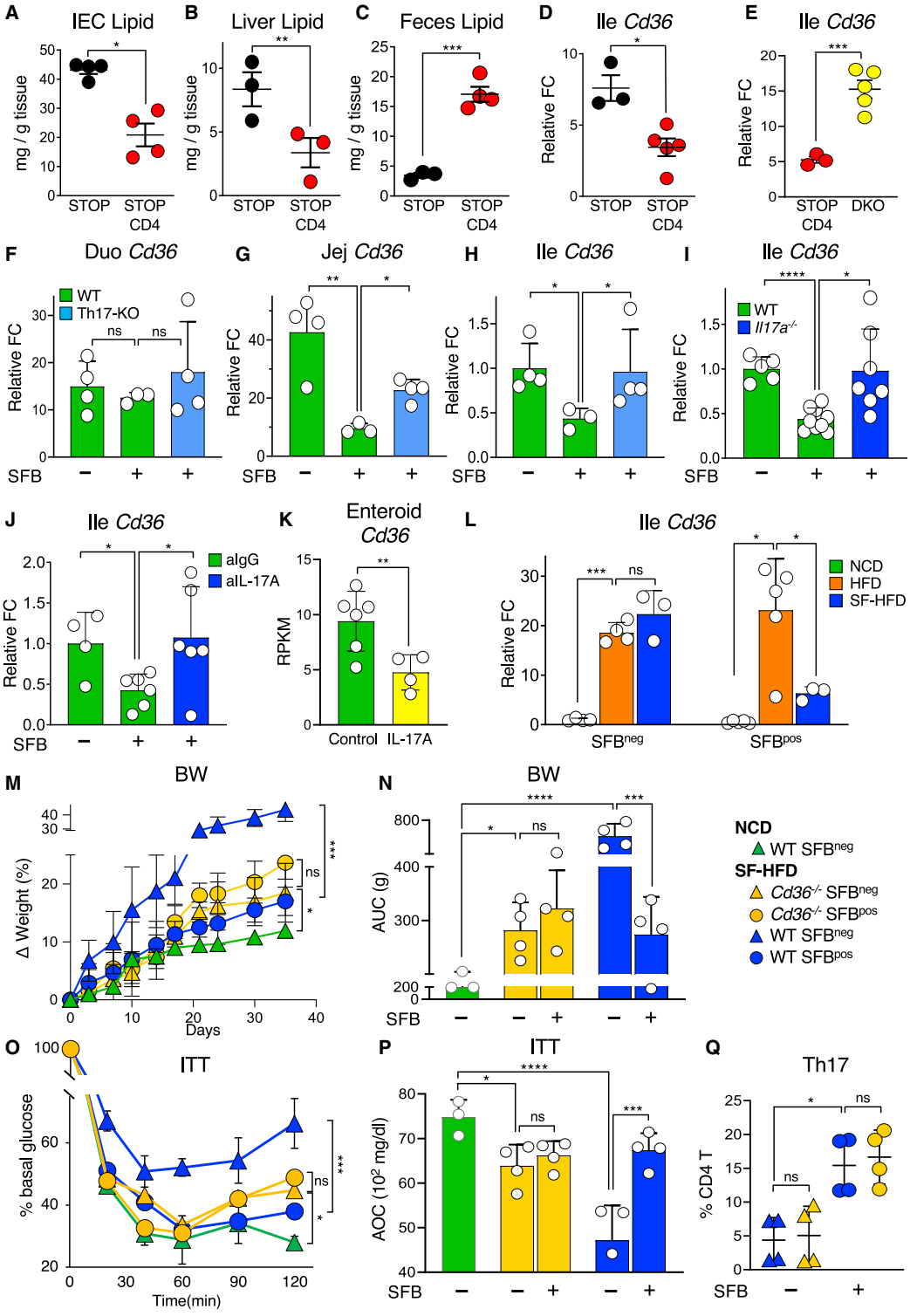

(legend on next page)

This protection was relatively mild at the 4-week timepoint we examined but could be more significant long-term. We also show that maintenance of commensal Th17 cells in ILC3-deficient mice confers lasting protection. Moreover, ILC3 function, likely through IL-22 production, was required for sugar-mediated expansion of *Frod* and consequent loss of SFB and protective Th17 cells. Therefore, ILC3 can counteract the protective role of Th17 cells and, in such context, contribute to the pathogenic effects of HFD. Thus, the effects of ILC3, and by extension IL-22, on complex phenotypes, such as metabolic syndrome, are dependent on microbiota composition and the presence of Th17 cells, and this should be taken into consideration when interpreting experimental results or designing cytokine-based therapies.

We demonstrate that commensal microbiota can protect from metabolic syndrome through modulation of intestinal T cell homeostasis. Our results are consistent with previous studies suggesting intestinal Th17 cells protect from metabolic syndrome (Garidou et al., 2015; Hong et al., 2017). Here we demonstrate that protective Th17 cells are commensal-specific and are depleted during DIO by diet-induced depletion of Th17-inducing microbiota. We also identify sucrose as a dietary component that is sufficient to deplete Th17-inducing bacteria and Th17 cells. Dietary sugar is considered detrimental for metabolic disease; however, the underlying mechanisms are not well understood (Macdonald, 2016; Stanhope, 2016). Here we propose a conceptually distinct mechanism in which sucrose does not directly drive metabolic syndrome but counteracts the protective function of intestinal immune cells by modulating intestinal microbiota. Sucrose and fructose intake have been associated with increase in intestinal inflammation and inflammatory bowel disease (Laffin et al., 2019; Racine et al., 2016). Our results suggest that dietary sugar can increase the inflammatory tone of the intestine indirectly by depleting intestinal microbes that maintain tissue homeostasis. Elimination of sugar from HFD protected mice from disease by preserving commensal Th17 cells. Importantly, SF-HFD exerted protection only in the presence of Th17 cell-inducing microbiota and provided no benefit in the absence of commensal Th17 cells. Therefore, dietary interventions may only provide benefit if appropriate microbiota-regulated immune mechanisms are also in place. It is expected that individual variations in such mechanisms will affect the success of diet-based therapies and should be taken into consideration.

We find that dietary sugar depletes SFB indirectly by expanding other gut bacteria. We identify *Faecalibaculum rodentium* as one such microbe and show that it is sufficient to displace SFB and decrease SFB-induced Th17 cells. *Frod* colonizes the mucosal surface of ileum and colon (Zagato et al., 2020) and as we report here can be found in close proximity to SFB in gnotobiotic animals, suggesting that displacement could be mediated by direct interactions between the two species. This is also supported by the fact that in our colony, *Frod* is present in low abundance in NCD-fed SPF mice without displacing SFB. SFB displacement required expansion of *Frod* by sugar or relatively large amounts of *Frod* in gnotobiotic animals, which suggests that an abundance threshold is required for *Frod* to displace SFB. The mechanisms by which *Frod* inhibits SFB will be important to investigate in the future. An equally important question is whether other microbes have similar effects. We consider it likely that other commensals can also negatively affect Th17 cell-inducing microbiota. Our results demonstrate that dietary effects on immunoregulatory microbes can be mediated by microbe-microbe interactions.

Dietary lipids are major drivers of the inflammatory effects of HFD, including barrier leakage, endotoxemia, and type 1 inflammation (Basson et al., 2020; Khan et al., 2021; Zmora et al., 2017). However, the detailed mechanisms involved and the relative contribution of these mechanisms to metabolic disease are not currently known. We find that commensal Th17 cells can decrease lipid absorption, and this will likely affect inflammatory phenotypes in the intestine and adipose tissue. Indeed, in most of our experiments, the presence of commensal Th17 cells was accompanied by decrease in Th1 intestinal responses and bacterial translocation. Decrease in Th1 inflammation, including intestinal Th1 inflammation, improves obesity related metabolic phenotypes (Luck et al., 2015; Wong et al., 2011) and can contribute to the protective function of commensal Th17 cells. At the same time, commensal Th17 cells may also influence

Figure 7. Commensal Th17 cells prevent metabolic syndrome by regulating intestinal lipid absorption

(A–C) Total lipid contents in IEC (A), liver (B), and feces (C) of STOP and STOP CD4 mice fed HFD for 5 weeks. Data from two independent experiments. n = 4 mice/group.

(D) *Cd36* transcripts in ileum IEC from STOP and STOP/CD4 mice fed HFD for 4 weeks. Data from two independent experiments. n = 3–5 mice/group.

(E) *Cd36* transcripts in ileum IEC from STOP/CD4 mice and TCRβ-KO STOP/CD4 mice (DKO) fed HFD for 5 weeks. Data from two independent experiments. n = 3–5 mice/group.

(F–H) *Cd36* transcripts in IEC from the duodenum (F), jejunum(G), and ileum (H) of WT mice and Th17 cell-deficient RORγt^{flox}/CD4-Cre mice under NCD. Data from two independent experiments. n = 4 mice/group.

(I) *Cd36* transcripts in ileum IEC of IL-17A-deficient mice and corresponding WT littermates. Data from two independent experiments. n = 5–8 mice/group.

(J) *Cd36* transcripts in ileum IEC of WT mice treated with anti-IL-17A neutralizing or control IgG antibody. Data from two independent experiments. n = 4–6 mice/group.

(K) *Cd36* transcripts in terminal ileum enteroids treated with rIL-17A *in vitro* (analysis of RNA-seq data from Kumar et al., 2016).

(L) *Cd36* transcripts in ileum IEC from SFB-negative and SFB-gavaged WT mice fed NCD, HFD, and SF-HFD for 10 days. Data combined from two independent experiments. n = 3–5 mice/group.

(M–P) Body weight change (L and M) and insulin tolerance test on day 28 (N and O) of WT and *Cd36*$^{-/-}$ mice fed SF-HFD for 4 weeks. Data from one out of two independent experiments. n = 4 mice/group.

(Q) IL-17^{+} Th17 cells in the SI LP of WT and *Cd36*$^{-/-}$ mice fed SF-HFD for 5 weeks. Proportion of TCRβ^{+}CD4^{+} cells. Data from one out of two independent experiments. n = 4 mice/group.

See also Figure S7.

low-grade inflammation independently of lipid absorption, for example by controlling local intestinal inflammation. Indeed, SFB-induced Th17 cells differ significantly from pathogen-induced inflammatory Th17 cells and may participate in maintenance of intestinal immune homeostasis (Khan et al., 2021; Omenetti et al., 2019; Wu et al., 2020). Therefore, commensal Th17 cells may possess additional mechanisms of protection from metabolic disease.

CD36 is a critical regulator of lipid absorption and fat metabolism and CD36 deficiency is associated with resistance to obesity and metabolic syndrome (Cai et al., 2012; Febbraio et al., 1999; Hajri et al., 2007; Kennedy and Kashyap, 2011; Yang et al., 2018). Microbiota can promote host lipid absorption by enhancing epithelial CD36 (Wang et al., 2017). Microbiota can also restrain lipid absorption and prevent obesity by decreasing intestinal epithelial CD36 (Petersen et al., 2019). We find that commensal Th17 cells protect from DIO and metabolic syndrome by decreasing IEC expression of CD36 and intestinal lipid absorption in an IL-17-dependent manner. CD36 is expressed on multiple cell types and has pleiotropic roles in metabolic disease (Chen et al., 2022; Pepino et al., 2014). Whether Th17 cell mediated regulation of CD36 can protect through additional mechanisms requires further study.

Our work describes an intricate network of interactions between dietary components, microbiota, and intestinal immune cells that regulates metabolic conditions such as DIO, metabolic syndrome, and T2D. Our findings also suggest that the effects of dietary and immune interventions on metabolic conditions are not universal. Future precision medicine therapeutic approaches should take into account individual variations of immunomodulatory microbiota.

Limitations of the study

Our study was limited to early stages of DIO and changes in intestinal environment. Adipose tissue inflammation was not evident at the early time points we examined; however, the protective effects of commensal Th17 cells were further re-enforced at 9 weeks and are, therefore, long-lasting. Nevertheless, the long-term effects and mechanisms of Th17 cell protection in systemic disease will be important to examine in the future. Also, although we demonstrate clear role for sugar and *Faecalibacilum rodentium* in opposing commensal Th17 cells, other dietary and microbiota components may have similar effects. Finally, our study was limited to animal models. We find that reported Th17-inducing microbes are also negatively affected by metabolic disease and sugar consumption in adult humans. Whether these, or other, microbes can induce intestinal Th17 cells with protective functions in metabolic disease in human patients will be important to investigate.

STAR★METHODS

Detailed methods are provided in the online version of this paper and include the following:

SUPPLEMENTAL INFORMATION

Supplemental information can be found online at https://doi.org/10.1016/j.cell.2022.08.005.

ACKNOWLEDGMENTS

We thank Guilhermina Carriche and Iliyan Iliev for help with gnotobiotic experiments. We thank members of the Ivanov lab for technical help. We thank Sridhar Radhakrishan from ResearchDiets for custom diet design. This work was supported by funding from NIH (DK098378, AI144808, AI163069, AI146817) and Burroughs Wellcome Fund (PATH1019125) to I.I.I. and NIH (DK093674, DK113375) to D.M. Y.K was supported by fellowships from MSD Life Science Foundation, the Russell BerrieFoundation, and the Naomi Berrie Diabetes Center at CUIMC. K.H. is funded by a Grant-in-Aid for Specially Promoted Research from the Japan Society for the Promotion of Science (20H05627). H.H.W. acknowledges funding from NSF (MCB-2025515), NIH (R01AI132403, R01DK118044, R01EB031935), Burroughs Wellcome Fund (PATH1016691), and the Irma T. Hirschl Trust.

AUTHOR CONTRIBUTIONS

Conceptualization, Y.K. and I.I.I.; methodology, Y.K., Y.H., and I.I.I.; software, Y.H. and H.H.W.; formal analysis, Y.K. and Y.H.; investigation, Y.K., M.E., Y.H., A.M.B., L.P.A., T.T., K.A., and M.S.L.; resources, H.H.W., D.M., K.H., and I.I.I.; data curation, Y.K., M.E., and Y.H.; writing—original draft, Y.K. and I.I.I.; writing — review and editing, M.E., Y.K., Y.H., A.M.B., S.L.R., D.M., K.H., and I.I.I.; supervision, S.L.R., H.H.W., D.M., K.H., and I.I.I.; funding acquisition, Y.K. and I.I.I.

DECLARATION OF INTERESTS

H.H.W. is a scientific advisor of SNIPR Biome, Kingdom Supercultures, and Fitbiomics, who were not involved in the study. K.H. is a scientific advisory board member of Vedanta Biosciences and 4BIO CAPITAL, who were not involved in the study.

Received: February 13, 2022
Revised: June 15, 2022
Accepted: August 4, 2022
Published: August 29, 2022

REFERENCES

The GBD 2015 Obesity Collaborators, Afshin, A., Forouzanfar, M.H., Reitsma, M.B., Sur, P., Estep, K., Lee, A., Marczak, L., Mokdad, A.H., Moradi-Lakeh, M., et al. (2017). Health Effects of Overweight and Obesity in 195 Countries over 25 Years. N. Engl. J. Med. *377*, 13–27. https://doi.org/10.1056/nejmoa1614362.

Alexander, M., Ang, Q.Y., Nayak, R.R., Bustion, A.E., Sandy, M., Zhang, B., Upadhyay, V., Pollard, K.S., Lynch, S.V., and Turnbaugh, P.J. (2022). Human gut bacterial metabolism drives Th17 activation and colitis. Cell host & microbe *30*, 17–30.e9. e19. https://doi.org/10.1016/j.chom.2021.11.001.

Atarashi, K., Nishimura, J., Shima, T., Umesaki, Y., Yamamoto, M., Onoue, M., Yagita, H., Ishii, N., Evans, R., Honda, K., and Takeda, K. (2008). ATP drives lamina propria T(H)17 cell differentiation. Nature *455*, 808–812. https://doi.org/10.1038/nature07240.

Atarashi, K., Tanoue, T., Ando, M., Kamada, N., Nagano, Y., Narushima, S., Suda, W., Imaoka, A., Setoyama, H., Nagamori, T., et al. (2015). Th17 Cell Induction by Adhesion of Microbes to Intestinal Epithelial Cells. Cell *163*, 367–380. https://doi.org/10.1016/j.cell.2015.08.058.

Barman, M., Unold, D., Shifley, K., Amir, E., Hung, K., Bos, N., and Salzman, N. (2008). Enteric salmonellosis disrupts the microbial ecology of the murine gastrointestinal tract. Infect. Immun. *76*, 907–915. https://doi.org/10.1128/iai.01432-07.

Basson, A.R., Chen, C., Sagl, F., Trotter, A., Bederman, I., Gomez-Nguyen, A., Sundrud, M.S., Ilic, S., Cominelli, F., and Rodriguez-Palacios, A. (2020). Regulation of Intestinal Inflammation by Dietary Fats. Front. Immunol. *11*, 604989. https://doi.org/10.3389/fimmu.2020.604989.

Biton, M., Haber, A.L., Rogel, N., Burgin, G., Beyaz, S., Schnell, A., Ashenberg, O., Su, C.W., Smillie, C., Shekhar, K., et al. (2018). T Helper Cell Cytokines Modulate Intestinal Stem Cell Renewal and Differentiation. Cell *175*, 1307–1320.e22. https://doi.org/10.1016/j.cell.2018.10.008.

Bravo, S., Lowndes, J., Sinnett, S., Yu, Z., and Rippe, J. (2013). Consumption of sucrose and high-fructose corn syrup does not increase liver fat or ectopic fat deposition in muscles. Appl Physiol Nutr Metab *38*, 681–688. https://doi.org/10.1139/apnm-2012-0322.

Buttet, M., Poirier, H., Traynard, V., Gaire, K., Tran, T.T.T., Sundaresan, S., Besnard, P., Abumrad, N.A., and Niot, I. (2016). Deregulated Lipid Sensing by Intestinal CD36 in Diet-Induced Hyperinsulinemic Obese Mouse Model. PLoS One *11*, e0145626. https://doi.org/10.1371/journal.pone.0145626.

Cai, L., Wang, Z., Ji, A., Meyer, J.M., and van der Westhuyzen, D.R. (2012). Scavenger receptor CD36 expression contributes to adipose tissue inflammation and cell death in diet-induced obesity. PLoS One *7*, e36785. https://doi.org/10.1371/journal.pone.0036785.

Cani, P.D., Bibiloni, R., Knauf, C., Waget, A., Neyrinck, A.M., Delzenne, N.M., and Burcelin, R. (2008). Changes in gut microbiota control metabolic endotoxemia-induced inflammation in high-fat diet-induced obesity and diabetes in mice. Diabetes *57*, 1470–1481. https://doi.org/10.2337/db07-1403.

Chen, M., Yang, Y., Braunstein, E., Georgeson, K.E., and Harmon, C.M. (2001). Gut expression and regulation of FAT/CD36: possible role in fatty acid transport in rat enterocytes. Am. J. Physiol. Endocrinol. Metab. *281*, E916–E923. https://doi.org/10.1152/ajpendo.2001.281.5.e916.

Chen, Y., Zhang, J., Cui, W., and Silverstein, R.L. (2022). CD36, a signaling receptor and fatty acid transporter that regulates immune cell metabolism and fate. J. Exp. Med. *219*, e20211314. https://doi.org/10.1084/jem.20211314.

Choi, G.B., Yim, Y.S., Wong, H., Kim, S., Kim, H., Kim, S.V., Hoeffer, C.A., Littman, D.R., and Huh, J.R. (2016). The maternal interleukin-17a pathway in mice promotes autism-like phenotypes in offspring. Science *351*, 933–939. https://doi.org/10.1126/science.aad0314.

Dalmas, E., Venteclef, N., Caer, C., Poitou, C., Cremer, I., Aron-Wisnewsky, J., Lacroix-Desmazes, S., Bayry, J., Kaveri, S.V., Clément, K., et al. (2014). T cell-derived IL-22 amplifies IL-1β-driven inflammation in human adipose tissue: relevance to obesity and type 2 diabetes. Diabetes *63*, 1966–1977. https://doi.org/10.2337/db13-1511.

de Wit, N., Derrien, M., Bosch-Vermeulen, H., Oosterink, E., Keshtkar, S., Duval, C., de Vogel-van den Bosch, J., Kleerebezem, M., Muller, M., and van der Meer, R. (2012). Saturated fat stimulates obesity and hepatic steatosis and affects gut microbiota composition by an enhanced overflow of dietary fat to the distal intestine. Am. J. Physiol. Gastrointest. Liver Physiol. *303*, G589–G599. https://doi.org/10.1152/ajpgi.00488.2011.

Edgar, R.C. (2010). Search and clustering orders of magnitude faster than BLAST. Bioinformatics *26*, 2460–2461. https://doi.org/10.1093/bioinformatics/btq461.

Fabbrini, E., Cella, M., McCartney, S.A., Fuchs, A., Abumrad, N.A., Pietka, T.A., Chen, Z., Finck, B.N., Han, D.H., Magkos, F., et al. (2013). Association between specific adipose tissue CD4+ T-cell populations and insulin resistance in obese individuals. Gastroenterology *145*, 366–374.e3. e361-363. https://doi.org/10.1053/j.gastro.2013.04.010.

Farkas, A.M., Panea, C., Goto, Y., Nakato, G., Galan-Diez, M., Narushima, S., Honda, K., and Ivanov, I.I. (2015). Induction of Th17 cells by segmented filamentous bacteria in the murine intestine. J. Immunol. Methods *421*, 104–111. https://doi.org/10.1016/j.jim.2015.03.020.

Febbraio, M., Abumrad, N.A., Hajjar, D.P., Sharma, K., Cheng, W., Pearce, S.F.A., and Silverstein, R.L. (1999). A null mutation in murine CD36 reveals an important role in fatty acid and lipoprotein metabolism. J. Biol. Chem. *274*, 19055–19062. https://doi.org/10.1074/jbc.274.27.19055.

Garidou, L., Pomie, C., Klopp, P., Waget, A., Charpentier, J., Aloulou, M., Giry, A., Serino, M., Stenman, L., Lahtinen, S., et al. (2015). The gut microbiota regulates intestinal CD4 T cells expressing RORγt and controls metabolic disease. Cell Metab *22*, 100–112. https://doi.org/10.1016/j.cmet.2015.06.001.

Di Angelantonio, E., Bhupathiraju, S.N., Wormser, D., Gao, P., Kaptoge, S., de Gonzalez, A.B., Cairns, B.J., Huxley, R., Jackson, C.L., Joshy, G., et al. (2016). Body-mass index and all-cause mortality: individual-participant-data meta-analysis of 239 prospective studies in four continents. Lancet *388*, 776–786. https://doi.org/10.1016/s0140-6736(16)30175-1.

Goto, Y., Panea, C., Nakato, G., Cebula, A., Lee, C., Diez, M., Laufer, T., Ignatowicz, L., and Ivanov, I. (2014). Segmented filamentous bacteria antigens presented by intestinal dendritic cells drive mucosal Th17 cell differentiation. Immunity *40*, 594–607. https://doi.org/10.1016/j.immuni.2014.03.005.

Hajri, T., Hall, A.M., Jensen, D.R., Pietka, T.A., Drover, V.A., Tao, H., Eckel, R., and Abumrad, N.A. (2007). CD36-facilitated fatty acid uptake inhibits leptin production and signaling in adipose tissue. Diabetes *56*, 1872–1880. https://doi.org/10.2337/db06-1699.

Hao, Y., Hao, S., Andersen-Nissen, E., Mauck, W.M., 3rd, Zheng, S., Butler, A., Lee, M.J., Wilk, A.J., Darby, C., Zager, M., et al. (2021). Integrated analysis of multimodal single-cell data. Cell *184*, 3573–3587.e29. https://doi.org/10.1016/j.cell.2021.04.048.

Honda, K., and Littman, D.R. (2016). The microbiota in adaptive immune homeostasis and disease. Nature *535*, 75–84. https://doi.org/10.1038/nature18848.

Hong, C.P., Park, A., Yang, B.G., Yun, C.H., Kwak, M.J., Lee, G.W., Kim, J.H., Jang, M.S., Lee, E.J., Jeun, E.J., et al. (2017). Gut-Specific Delivery of T-Helper 17 Cells Reduces Obesity and Insulin Resistance in Mice. Gastroenterology *152*, 1998–2010. https://doi.org/10.1053/j.gastro.2017.02.016.

Hueber, W., Sands, B.E., Lewitzky, S., Vandemeulebroecke, M., Reinisch, W., Higgins, P.D.R., Wehkamp, J., Feagan, B.G., Yao, M.D., Karczewski, M., et al. (2012). Secukinumab, a human anti-IL-17A monoclonal antibody, for moderate to severe Crohn's disease: unexpected results of a randomised, double-blind placebo-controlled trial. Gut *61*, 1693–1700. https://doi.org/10.1136/gutjnl-2011-301668.

Ivanov, I.I., Atarashi, K., Manel, N., Brodie, E.L., Shima, T., Karaoz, U., Wei, D., Goldfarb, K.C., Santee, C.A., Lynch, S.V., et al. (2009). Induction of intestinal Th17 cells by segmented filamentous bacteria. Cell *139*, 485–498. https://doi.org/10.1016/j.cell.2009.09.033.

Ivanov, , II, Tuganbaev, T., Skelly, A.N., and Honda, K. (2022). T Cell Responses to the Microbiota. Annual Review of Immunology.

Ji, B.W., Sheth, R.U., Dixit, P.D., Huang, Y., Kaufman, A., Wang, H.H., and Vitkup, D. (2019). Quantifying spatiotemporal variability and noise in absolute microbiota abundances using replicate sampling. Nat. Methods *16*, 731–736. https://doi.org/10.1038/s41592-019-0467-y.

Johnson, A.J., Vangay, P., Al-Ghalith, G.A., Hillmann, B.M., Ward, T.L., Shields-Cutler, R.R., Kim, A.D., Shmagel, A.K., Syed, A.N., Walter, J., et al. (2019). Daily Sampling Reveals Personalized Diet-Microbiome Associations in Humans. Cell host & microbe *25*, 789–802.e5. https://doi.org/10.1016/j.chom.2019.05.005.

Johnson, R.J., Nakagawa, T., Sanchez-Lozada, L.G., Shafiu, M., Sundaram, S., Le, M., Ishimoto, T., Sautin, Y.Y., and Lanaspa, M.A. (2013). Sugar, uric acid, and the etiology of diabetes and obesity. Diabetes *62*, 3307–3315. https://doi.org/10.2337/db12-1814.

Kawano, Y., Nakae, J., Watanabe, N., Kikuchi, T., Tateya, S., Tamori, Y., Kaneko, M., Abe, T., Onodera, M., and Itoh, H. (2016). Colonic Pro-inflammatory Macrophages Cause Insulin Resistance in an Intestinal Ccl2/Ccr2-Dependent Manner. Cell Metab *24*, 295–310. https://doi.org/10.1016/j.cmet.2016.07.009.

Kennedy, D.J., and Kashyap, S.R. (2011). Pathogenic role of scavenger receptor CD36 in the metabolic syndrome and diabetes. Metab. Syndr. Relat. Disord. *9*, 239–245. https://doi.org/10.1089/met.2011.0003.

Khan, S., Luck, H., Winer, S., and Winer, D.A. (2021). Emerging concepts in intestinal immune control of obesity-related metabolic disease. Nat. Commun. *12*, 2598. https://doi.org/10.1038/s41467-021-22727-7.

Klose, C.S.N., and Artis, D. (2016). Innate lymphoid cells as regulators of immunity, inflammation and tissue homeostasis. Nat. Immunol. *17*, 765–774. https://doi.org/10.1038/ni.3489.

Kraus, D., Yang, Q., and Kahn, B. (2015). Lipid Extraction from Mouse Feces. Bio-Protoc. *5*, e1375. https://doi.org/10.21769/bioprotoc.1375.

Kumar, P., Monin, L., Castillo, P., Elsegeiny, W., Horne, W., Eddens, T., Vikram, A., Good, M., Schoenborn, A.A., Bibby, K., et al. (2016). Intestinal Interleukin-17 Receptor Signaling Mediates Reciprocal Control of the Gut Microbiota and Autoimmune Inflammation. Immunity *44*, 659–671. https://doi.org/10.1016/j.immuni.2016.02.007.

Ladinsky, M.S., Araujo, L.P., Zhang, X., Veltri, J., Galan-Diez, M., Soualhi, S., Lee, C., Irie, K., Pinker, E.Y., Narushima, S., et al. (2019). Endocytosis of commensal antigens by intestinal epithelial cells regulates mucosal T cell homeostasis. Science *363*, eaat4042. https://doi.org/10.1126/science.aat4042.

Laffin, M., Fedorak, R., Zalasky, A., Park, H., Gill, A., Agrawal, A., Keshteli, A., Hotte, N., and Madsen, K.L. (2019). A high-sugar diet rapidly enhances susceptibility to colitis via depletion of luminal short-chain fatty acids in mice. Sci. Rep. *9*, 12294. https://doi.org/10.1038/s41598-019-48749-2.

Langmead, B., and Salzberg, S.L. (2012). Fast gapped-read alignment with Bowtie 2. Nat. Methods *9*, 357–359. https://doi.org/10.1038/nmeth.1923.

Lee, J., Tato, C., Joyce-Shaikh, B., Gulen, M., Cayatte, C., Chen, Y., Blumenschein, W., Judo, M., Ayanoglu, G., McClanahan, T., et al. (2015). Interleukin-23-Independent IL-17 Production Regulates Intestinal Epithelial Permeability. Immunity *43*, 727–738. https://doi.org/10.1016/j.immuni.2015.09.003.

Ley, R.E., Turnbaugh, P.J., Klein, S., and Gordon, J.I. (2006). Microbial ecology: human gut microbes associated with obesity. Nature *444*, 1022–1023. https://doi.org/10.1038/4441022a.

Luck, H., Tsai, S., Chung, J., Clemente-Casares, X., Ghazarian, M., Revelo, X., Lei, H., Luk, C., Shi, S., Surendra, A., et al. (2015). Regulation of obesity-related insulin resistance with gut anti-inflammatory agents. Cell Metab *21*, 527–542. https://doi.org/10.1016/j.cmet.2015.03.001.

Lugli, G.A., Duranti, S., Albert, K., Mancabelli, L., Napoli, S., Viappiani, A., Anzalone, R., Longhi, G., Milani, C., Turroni, F., et al. (2019). Unveiling Genomic Diversity among Members of the Species Bifidobacterium pseudolongum, a Widely Distributed Gut Commensal of the Animal Kingdom. Appl. Environ. Microbiol. *85*, e03065-18. https://doi.org/10.1128/aem.03065-18.

Macdonald, I.A. (2016). A review of recent evidence relating to sugars, insulin resistance and diabetes. Eur. J. Nutr. *55*, 17–23. https://doi.org/10.1007/s00394-016-1340-8.

Malik, V.S., Popkin, B.M., Bray, G.A., Despres, J.P., and Hu, F.B. (2010). Sugar-sweetened beverages, obesity, type 2 diabetes mellitus, and cardiovascular disease risk. Circulation *121*, 1356–1364. https://doi.org/10.1161/circulationaha.109.876185.

Martin, M. (2011). Cutadapt removes adapter sequences from high-throughput sequencing reads. EMBnetjournal *17*, 10. https://doi.org/10.14806/ej.17.1.200.

Nauli, A.M., Nassir, F., Zheng, S., Yang, Q., Lo, C., Vonlehmden, S.B., Lee, D., Jandacek, R.J., Abumrad, N.A., and Tso, P. (2006). CD36 is important for chylomicron formation and secretion and may mediate cholesterol uptake in the proximal intestine. Gastroenterology *131*, 1197–1207. https://doi.org/10.1053/j.gastro.2006.08.012.

O'Connor Jr, W., Kamanaka, M., Booth, C.J., Town, T., Nakae, S., Iwakura, Y., Kolls, J.K., and Flavell, R.A. (2009). A protective function for interleukin 17A in T cell-mediated intestinal inflammation. Nat. Immunol. *10*, 603–609. https://doi.org/10.1038/ni.1736.

Omenetti, S., Bussi, C., Metidji, A., Iseppon, A., Lee, S., Tolaini, M., Li, Y., Kelly, G., Chakravarty, P., Shoaie, S., et al. (2019). The Intestine Harbors Functionally Distinct Homeostatic Tissue-Resident and Inflammatory Th17 Cells. Immunity *51*, 77–89.e6. e76. https://doi.org/10.1016/j.immuni.2019.05.004.

Pedersen, H.K., Gudmundsdottir, V., Nielsen, H.B., Hyotylainen, T., Nielsen, T., Jensen, B.A.H., Forslund, K., Hildebrand, F., Prifti, E., Falony, G., et al. (2016). Human gut microbes impact host serum metabolome and insulin sensitivity. Nature *535*, 376–381. https://doi.org/10.1038/nature18646.

Pepino, M.Y., Kuda, O., Samovski, D., and Abumrad, N.A. (2014). Structure-function of CD36 and importance of fatty acid signal transduction in fat metabolism. Annu. Rev. Nutr. *34*, 281–303. https://doi.org/10.1146/annurev-nutr-071812-161220.

Perez, M.M., Martins, L.M.S., Dias, M.S., Pereira, C.A., Leite, J.A., Goncalves, E.C.S., de Almeida, P.Z., de Freitas, E.N., Tostes, R.C., Ramos, S.G., et al. (2019). Interleukin-17/interleukin-17 receptor axis elicits intestinal neutrophil migration, restrains gut dysbiosis and lipopolysaccharide translocation in high-fat diet-induced metabolic syndrome model. Immunology *156*, 339–355. https://doi.org/10.1111/imm.13028.

Petersen, C., Bell, R., Klag, K.A., Lee, S.H., Soto, R., Ghazaryan, A., Buhrke, K., Ekiz, H.A., Ost, K.S., Boudina, S., et al. (2019). T cell-mediated regulation of the microbiota protects against obesity. Science *365*, eaat9351. https://doi.org/10.1126/science.aat9351.

Racine, A., Carbonnel, F., Chan, S.S.M., Hart, A.R., Bueno-de-Mesquita, H.B., Oldenburg, B., van Schaik, F.D.M., Tjonneland, A., Olsen, A., Dahm, C.C., et al. (2016). Dietary Patterns and Risk of Inflammatory Bowel Disease in Europe: Results from the EPIC Study. Inflamm. Bowel Dis. *22*, 345–354. https://doi.org/10.1097/mib.0000000000000638.

Sano, T., Huang, W., Hall, J., Yang, Y., Chen, A., Gavzy, S., Lee, J.Y., Ziel, J.W., Miraldi, E., Domingos, A., et al. (2015). An IL-23R/IL-22 Circuit Regulates Epithelial Serum Amyloid A to Promote Local Effector Th17 Responses. Cell *163*, 381–393. https://doi.org/10.1016/j.cell.2015.08.061.

Sasaki, T., Moro, K., Kubota, T., Kubota, N., Kato, T., Ohno, H., Nakae, S., Saito, H., and Koyasu, S. (2019). Innate Lymphoid Cells in the Induction of Obesity. Cell Rep. *28*, 202–217.e7. e207. https://doi.org/10.1016/j.celrep.2019.06.016.

Silverstein, R.L., and Febbraio, M. (2009). CD36, a scavenger receptor involved in immunity, metabolism, angiogenesis, and behavior. Sci. Signal. *2*, re3. https://doi.org/10.1126/scisignal.272re3.

Stanhope, K.L. (2016). Sugar consumption, metabolic disease and obesity: The state of the controversy. Crit. Rev. Clin. Lab Sci. *53*, 52–67. https://doi.org/10.3109/10408363.2015.1084990.

Tait Wojno, E.D., and Artis, D. (2016). Emerging concepts and future challenges in innate lymphoid cell biology. J. Exp. Med. *213*, 2229–2248. https://doi.org/10.1084/jem.20160525.

Tan, T.G., Sefik, E., Geva-Zatorsky, N., Kua, L., Naskar, D., Teng, F., Pasman, L., Ortiz-Lopez, A., Jupp, R., Wu, H.J.J., et al. (2016). Identifying species of symbiont bacteria from the human gut that, alone, can induce intestinal Th17 cells in mice. Proceedings of the National Academy of Sciences of the United States of America *113*, E8141–E8150. https://doi.org/10.1073/pnas.1617460113.

Tilg, H., Zmora, N., Adolph, T.E., and Elinav, E. (2020). The intestinal microbiota fuelling metabolic inflammation. Nat. Rev. Immunol. *20*, 40–54. https://doi.org/10.1038/s41577-019-0198-4.

Turnbaugh, P.J., Backhed, F., Fulton, L., and Gordon, J.I. (2008). Diet-induced obesity is linked to marked but reversible alterations in the mouse distal gut microbiome. Cell Host Microbe *3*, 213–223. https://doi.org/10.1016/j.chom.2008.02.015.

Turnbaugh, P.J., Ley, R.E., Mahowald, M.A., Magrini, V., Mardis, E.R., and Gordon, J.I. (2006). An obesity-associated gut microbiome with increased capacity for energy harvest. Nature *444*, 1027–1031. https://doi.org/10.1038/nature05414.

Umesaki, Y., Okada, Y., Matsumoto, S., Imaoka, A., and Setoyama, H. (1995). Segmented filamentous bacteria are indigenous intestinal bacteria that activate intraepithelial lymphocytes and induce MHC class II molecules and fucosyl asialo GM1 glycolipids on the small intestinal epithelial cells in the ex-germ-free mouse. Microbiol. Immunol. *39*, 555–562. https://doi.org/10.1111/j.1348-0421.1995.tb02242.x.

Upadhyay, V., Poroyko, V., Kim, T.J., Devkota, S., Fu, S., Liu, D., Tumanov, A.V., Koroleva, E.P., Deng, L., Nagler, C., et al. (2012). Lymphotoxin regulates commensal responses to enable diet-induced obesity. Nat. Immunol. *13*, 947–953. https://doi.org/10.1038/ni.2403.

Vivier, E., Artis, D., Colonna, M., Diefenbach, A., Di Santo, J.P., Eberl, G., Koyasu, S., Locksley, R.M., McKenzie, A.N., Mebius, R.E., et al. (2018). Innate Lymphoid Cells: 10 Years On. Cell *174*, 1054–1066. https://doi.org/10.1016/j.cell.2018.07.017.

Wang, Q., Garrity, G.M., Tiedje, J.M., and Cole, J.R. (2007). Naive Bayesian classifier for rapid assignment of rRNA sequences into the new bacterial taxonomy. Appl. Environ. Microbiol. *73*, 5261–5267. https://doi.org/10.1128/aem.00062-07.

Wang, X., Ota, N., Manzanillo, P., Kates, L., Zavala-Solorio, J., Eidenschenk, C., Zhang, J., Lesch, J., Lee, W.P., Ross, J., et al. (2014). Interleukin-22 alleviates metabolic disorders and restores mucosal immunity in diabetes. Nature *514*, 237–241. https://doi.org/10.1038/nature13564.

Wang, Y., Kuang, Z., Yu, X., Ruhn, K.A., Kubo, M., and Hooper, L.V. (2017). The intestinal microbiota regulates body composition through NFIL3 and the circadian clock. Science *357*, 912–916. https://doi.org/10.1126/science.aan0677.

Ward, Z.J., Bleich, S.N., Cradock, A.L., Barrett, J.L., Giles, C.M., Flax, C., Long, M.W., and Gortmaker, S.L. (2019). Projected U.S. State-Level Prevalence of Adult Obesity and Severe Obesity. N. Engl. J. Med. *381*, 2440–2450. https://doi.org/10.1056/nejmsa1909301.

Winer, D., Luck, H., Tsai, S., and Winer, S. (2016). The Intestinal Immune System in Obesity and Insulin Resistance. Cell Metab *23*, 413–426. https://doi.org/10.1016/j.cmet.2016.01.003.

Wong, N., Fam, B.C., Cempako, G.R., Steinberg, G.R., Walder, K., Kay, T.W., Proietto, J., and Andrikopoulos, S. (2011). Deficiency in interferon-gamma results in reduced body weight and better glucose tolerance in mice. Endocrinology *152*, 3690–3699. https://doi.org/10.1210/en.2011-0288.

Wu, L., Hollinshead, K.E., Hao, Y., Au, C., Kroehling, L., Ng, C., Lin, W.Y., Li, D., Silva, H.M., Shin, J., et al. (2020). Niche-Selective Inhibition of Pathogenic Th17 Cells by Targeting Metabolic Redundancy. Cell *182*, 641–654.e20. https://doi.org/10.1016/j.cell.2020.06.014.

Yang, J., Park, K.W., and Cho, S. (2018). Inhibition of the CD36 receptor reduces visceral fat accumulation and improves insulin resistance in obese mice carrying the BDNF-Val66Met variant. J. Biol. Chem. *293*, 13338–13348. https://doi.org/10.1074/jbc.ra118.002405.

Yang, Y., Torchinsky, M.B., Gobert, M., Xiong, H., Xu, M., Linehan, J.L., Alonzo, F., Ng, C., Chen, A., Lin, X., et al. (2014). Focused specificity of intestinal TH17 cells towards commensal bacterial antigens. Nature *510*, 152–156. https://doi.org/10.1038/nature13279.

Zagato, E., Pozzi, C., Bertocchi, A., Schioppa, T., Saccheri, F., Guglietta, S., Fosso, B., Melocchi, L., Nizzoli, G., Troisi, J., et al. (2020). Endogenous murine microbiota member Faecalibaculum rodentium and its human homologue protect from intestinal tumour growth. Nat Microbiol *5*, 511–524. https://doi.org/10.1038/s41564-019-0649-5.

Zhang, H., DiBaise, J.K., Zuccolo, A., Kudrna, D., Braidotti, M., Yu, Y., Parameswaran, P., Crowell, M.D., Wing, R., Rittmann, B.E., and Krajmalnik-Brown, R. (2009). Human gut microbiota in obesity and after gastric bypass. Proc. Natl. Acad. Sci. U. S. A. *106*, 2365–2370. https://doi.org/10.1073/pnas.0812600106.

Zmora, N., Bashiardes, S., Levy, M., and Elinav, E. (2017). The Role of the Immune System in Metabolic Health and Disease. Cell Metab *25*, 506–521. https://doi.org/10.1016/j.cmet.2017.02.006.

Zou, J., Chassaing, B., Singh, V., Pellizzon, M., Ricci, M., Fythe, M.D., Kumar, M.V., and Gewirtz, A.T. (2018). Fiber-Mediated Nourishment of Gut Microbiota Protects against Diet-Induced Obesity by Restoring IL-22-Mediated Colonic Health. Cell Host Microbe *23*, 41–53.e4. e44. https://doi.org/10.1016/j.chom.2017.11.003.

STAR★METHODS

KEY RESOURCES TABLE

REAGENT or RESOURCE	SOURCE	IDENTIFIER
Antibodies		
Rat monoclonal anti-CD196(Ccr6) antibody, BV421	BD	#564736
American hamster anti CD3e, 145-2C11, FITC	eBioscience	#11-0031-82
Rat monoclonal anti CD4, RM4-5, APCCy7	Tonbo	#25-0042-U100
Rat monoclunal anti CD4, RM4-5, BV450	Tonbo	#75-0042-U100
CD4(L3T4) Micro-Beads, mouse	Miltenyi Biotec	#130-117-043
Rat monoclonal anti-CD8α, 53–6.7, PE	eBioscience	#12-0081-82
Rat anti CD11b, M1/70, APCCy7	Tonbo	#25-0112-U100
American Hamster monoclonal anti CD11c, N418, PECy7	eBioscience	#25-0114-82
Rat monoclonal anti CD24, M1/69, Pacific Blue	Tonbo	#48-0242-82
Mouse monoclonal anti CD45.1, A20, PE-Cy7	Tonbo	#60-0453-U100
Mouse monoclonal anti CD45.2, 104, PE	Tonbo	#50-0454-U100
Rat monoclonal anti CD45R/B220, RA3-6B2, Alexa Fluor 700	Tonbo	#103232
Rat monoclonal anti CD45R/B220, RA3-6B2, Biotin	Tonbo	#30-0452-U100
Mouse monoclonal anti CD64, X54-5/7.1, APC	Biolegend	#139305
Rat monoclonal anti CD206, C068C2, FITC	Biolegend	#141703
American Hamster monoclonal anti-gδTCR, GL-3,GL3 APC	eBioscience	#17-5711-82
Rat monoclonal anti F4/80, BM8.1, APC	Tonbo	#20-4801-U100
Mouse monoclonal anti FoxP3, 3G3, FITC	eBioscience	#11-5773-82
Fixable Viability Dye eFluor 506 (FVD)	Invitrogen	#65-0866-14
Rat monoclonal anti-mouse IFNγ, XMG1.2, APC	eBioscience	#17-7311-82
Rat monoclonal anti-mouse IL-17A, eBio17B7, PE	eBioscience	#12-7177-81
Goat monoclonal anti IL-22 antibody (POLY5164)	Biolegend	#516406
Rat monoclonal anti-mouse Ly6C. HK1.4. BV421	Biolegend	#128032
Rat monoclonal anti mouse Ly6G, 1A8, PE-Cy7	Tonbo	#60-1276-U100
Rat monoclunal anti mouse MHCII, M5/114.15.2, Alexa Fluor 710	Tonbo	#80-5321-U100
Rat monoclonal anti-mouse NKp46, 29A1.4, PerCP-Cyanine5.5	eBioscience	#46-3351-80
Rat monoclonal anti-mouse RORγt, PE	eBioscience	#12-6988-82
Streptavidin PE-eFluor 610 conjugated	eBioscience	#50-112-4814
American Hamster anti-TCRβ, H57-597	Biolegened	#47-0454-82
American Hamster monoclonal TCRβ, H57-597, PerCP-Cyanine5.5	Tonbo	#65-5921-U100
Rat monoclonal anti-Vβ14 TCR, 14-2(RUO), Biotin	BD Bioscience	#553257
Bacterial and virus strains		
Segmented Filamentous Bacteria (SFB)	Kenya Honda	(Umesaki et al., 1995)
Faecalibaculum rodentium (Frod) (PB1)	Kenya Honda	(Zagato et al., 2020)
Bifidobacterium pseudolongum (Bpl) (1B11)	Kenya Honda	(Atarashi et al., 2015)
Chemicals, peptides, and recombinant proteins		
In VivoMAb anti-mouse IL-17A neutralizing antibody (clone 17F3)	BioXcell,	#BE0173
In VivoMAb mouse IgG1 isotype control (MOPC-21)	BioXcell,	#BE0083

(*Continued on next page*)

Continued

REAGENT or RESOURCE	SOURCE	IDENTIFIER
In VivoMAb anti mouse CD4 Antibody (clone GK1.5.)	BioXcell	#BE0003-1
In VivoMAb rat IgG2b isotype control, anti keyhole limpet hemocyanin (clone LTF-2)	BioXcell	#BE0090
Corning Dispase, 100 mL	Corning (Fisher)	#354235
Roche Collagenase D 2.5g from C.histolyticum	Roche (Sigma)	#11088882001
Collagenase, type 1, powder	Gibco	#17018209
DNaseI from bovine pancreas, 1g	Sigma	DN-25
Sucrose (Crystaline/Certified ACS(S5-500-500g)	Fisher Chemical	#207263
Glucose (G8270-1kg. ≧99.5%)	SIGMA	#080M0175V
Galactose (BP656-500g)	Fisher bioreagents	#188103
Maltodextrin (419,680-100g) DE13.0–17.0	SIGMA-ALDRICH	#MKCL0273
Dextrose (D16-500, 500mg)	Fisher Scientific	#D16-500
Hanks' Balanced Salt solution (HBSS), 10X	CORNING	#36320020
HyClone™ RPMI 1640 Medium, Sterile, pH 7.0–7.4, With L-glutamine, Liquid	Cytiva	SH30028.LS
Sodium Bicarbonate	SIGMA	#46H02825
Percoll®, Sterile, pH 8.5–9.5, Liquid	Cytiva	17-0891-09
Fetal Bovine Serum, Qualified, USDA approved	Thermo Scientific	#10437028
HEPES(1M)	Thermofisher	#15630-080
Insulin human (recombinant yeast, 100mg)	Roche	#11376497001
Fisher Chemical BP176025 Ampicillin Sodium Salt	Fisher Scientific	#176025
Invitrogen ambion Sodium Acetate (3M), pH 5.5	Fisher scientific	#AM9740
Phenol/Chloro-form/Isoamyl alcohol (25:24:1), stabilized	Fisher Scientific	327,115,000
Ambion TRIzol reagent	Fisher Scientific	15-596-018
2-Propanol, ACS reagent, ≥99.5%	Sigma-Aldrich	#190764
Proteinase K	Lucigen	#MPRK092
Cell Trace Violet cell proliferation kit	Life Technologies	#34557
Ionomycin calcium salt from Streptomyces	Sigma-Aldrich	#10634
PMA, for use in molecular biology	Sigma-Aldrich	#P1585
Brefeldin A,from *Penicillium brefeldianum*, ≥99% (HPLC and TLC)	Sigma Aldrich	#B7651-5MG
BD cytofix/cytoperm Fixation and Permeabilization	Fisher scientific	#BDB554722
BD Perm/Wash Buffer	Fisher scientific	#BD554723
Foxp3/Transcription Factor Fix/Perm Concentrate (4X)	TONBO Biosciences	#TNB-1020-L050
Foxp3/Transcription Factor Staining Buffer Kit	TONBO Biosciences	#TNB-0607-KIT
Flow Cytometry Perm Buffer (10X)	TONBO Biosciences	#TNB-1213-L150
Critical commercial assays		
Neutral Lipid quantification, Fluorometric	Fisher cell Bio Lab	STA-617
Fluorometric Reagents (100×) 1 vial 200μL	Fisher cell Bio Lab	#261701
Lipid standard, 1 vial 100μL, 20 g/dL	Fisher cell Bio Lab	#261702
Qscript cDNA Super Mix, QuantaBio	VWR	#101414-108
2X Universal SYBR Green Fast qPCR Mix - 25 mL	ABclonal	#RK21203
Qubit dsDNA HS assay kit	ThermoFisher	#Q32581
Deposited data		
16S-V4 rRNA sequencing data NCBI BioProject database (http://www.ncbi.nlm.nih.gov/bioproject/)	This Study	accession ID PRJNA844056

(*Continued on next page*)

Continued

REAGENT or RESOURCE	SOURCE	IDENTIFIER
Experimental models: Organisms/strains		
C57BL/6J, Room RB15	The Jackson Laboratory	#000664
Ptprc (CD45.1)	The Jackson Laboratory	#002014
Cd4-Cre	The Jackson Laboratory	#022071
7B8 TCR Tg	The Jackson Laboratory	#027230
RORγ-flox	The Jackson Laboratory	#008771
IL-17A-GFP	The Jackson Laboratory	#018472
Il17a$^{-/-}$	The Jackson Laboratory	#016879
Cd36$^{-/-.}$	The Jackson Laboratory	#019006
Tcrβ$^{-/-}$	The Jackson Laboratory	#002118
RORγ-STOP mice	This Study	N/A
Oligonucleotides		
Cd36 F 5-ATGGGCTGTGATCGGAACTG-3′	This Study	N/A
Cd36 R-5-GTCTTCCCAATAAGCATGTCTCC-3′	This Study	N/A
Scd1 F 5-GAGTACCGCTGGCACATCAA-3′	This Study	N/A
Scd1 R-5-AAGCCCAAAGCTCAGCTACTC-3′	This Study	N/A
Npc1l1 F 5-CGGAACTCACAGGACTTTACAG-3′	This Study	N/A
Npc1l1 R-5-TGCTGGTAGAACACATTGGAG-3′	This Study	N/A
Fabp1 F 5-TCTCCGGCAAGTACCAATTG-3′	This Study	N/A
Fabp1 R-5-TTGATGTCCTTCCCTTTCTGG-3′	This Study	N/A
Fabp2 F 5-AGCTCGGTGTAAACTTTCCC-3′	This Study	N/A
*Fabp 2*R-5-TTCATTACCAGAAACCTCTCG G-3′	This Study	N/A
Reg3g F 5-CCTGATGCTCCTTTCTCAGG-3′	(Ladinsky et al., 2019)	N/A
Reg3g R-5-ATGTCCTGAGGGCCTCTTTT-3′	(Ladinsky et al., 2019)	N/A
Il17a F 5-GGACTCTCCACCGCAATGA-3′	(Atarashi et al., 2008)	N/A
Il17a R-5-GGCACTGAGCTTCCCAGATC-3′	(Atarashi et al., 2008)	N/A
Ifng F 5-CACGGCACAGTCATTGAAAG-3′	This Study	N/A
Ifng R-5-GCTGATGGCCTGATTGTCTT-3′	This Study	N/A
Tnfa F 5-GATCGGTCCCCAAAGGGATG-3′	This Study	N/A
Tnfa R-5-GTGGTTTGCTACGACGTGGG-3′	This Study	N/A
Lcn2 F 5-ATGTCACCTCCATCCTGGTCAG-3′	This Study	N/A
*Lcn 2*R-5-GCCACTTGCACATTGTAGCTCTG-3′	This Study	N/A
Cxcl1 F 5-TCCAGAGCTTGAAGGTGTTGCC-3′	This Study	N/A
Cxcl1 R-5-AACCAAGGGAGCTTCAGGGTCA-3′	This Study	N/A
SFB F 5-GACGCTGAGGCATGAGAGCAT-3′	(Barman et al., 2008)	N/A
SFB R-5-GACGGCACGGATTGTTATTCA-3′	(Barman et al., 2008)	N/A
UNI F 5-ACTCCTACGGGAGGCAGCAGT-3′	(Barman et al., 2008)	N/A
UNI R-5-ATTACCGCGGCTGCTGGC-3′	(Barman et al., 2008)	N/A
Frod F 5-CCGGGAATACGCTCTGGAAA-3′	(Zagato et al., 2020)	N/A
Frod R-5-GCCAACCAACTAATGCACCG-3′	(Zagato et al., 2020)	N/A
Bpl F 5-GCAAGTCTCCAATGTTGAGG-3′	(Lugli et al., 2019)	N/A
Bpl R-5-CTGTGCGGACGAGACGTAG-3′	(Lugli et al., 2019)	N/A
Gapdh F 5-CCTCGTCCCGTAGACAAAATG-3′	(Atarashi et al., 2008)	N/A
Gapdh R-5-TCTCCACTTTGCCACTGCAA-3′	(Atarashi et al., 2008)	N/A
Software and algorithms		
Flow jo_v10.6.2	BD	N/A
Cutadapt v2.1	N/A	N/A
Bowtie2 v2.3.4	N/A	N/A

(*Continued on next page*)

Continued

REAGENT or RESOURCE	SOURCE	IDENTIFIER
10X Genomics Cellranger toolkit v1.0.1	N/A	N/A
USEARCH v11.0.667	N/A	N/A
RDP classifier trained with 16S rRNA training set 18	N/A	N/A
Other		
BD LSR Fortessa Flow Cytometer	BD	N/A
Irradiated Normal Chow Diet, Lab diet 5061 (NCD, Pico-Vac Rodent Diet 20)	Lab Diet	#5061
Irradiated High Fat Diet (HFD)	Research Diets	#D12492i
Irradiated Sugar Free Starch Add High Fat Diet (SF-HFD)	Research Diets	#D19122401i
Irradiated Inulin supplemented High Fat Diet (HFD + Inulin)	Research Diets	#D13081106i
Irradiated Low Fat Diet (LFD)	Research Diets	#D12450Ji
Zirconia/Silica Beads 0.1mm	Fisher Scientific	#11079101z
Miltenyi Biotec, Inc. LS Columns 25/PK	Miltenyil Biotec	#130-042-401
LightCycler® 480 System	Roche	N/A
Fisherbrand Razor Blades	Fisher Schientific	#12640
Insulin Syringes with Permanently Attached Needles	BD	#329420
Cell Strainer, Individual Package, 40 um, blue	VWR	#76327-098
HPM-010 high-pressure freezing machine	Leica Microsystems, Vienna Austria	N/A
20% PhiX spike-in (Illumina FC-110-3001)	Illumina	FC-110-3001
Bead beater	Biospec	#1001
Beads cleanup	Beckman-Coulter	# A63881
AFS-2 freeze-substitution machine	Leica Microsystems	N/A
UC6 ultramicrotome	Leica Microsystems	N/A
Tecnai TF30ST-FEG transmission electron microscope (300 keV) equipped with a 2k x 2k CCD camera (XP1000).	Gatan Inc., Pleasanton CA	N/A

RESOURCE AVAILABILITY

Lead contact

Further information and requests for resources and reagents should be directed to and will be fulfilled by the lead contact, Ivaylo Ivanov (ii2137@cumc.columbia.edu).

Materials availability

RORγt-STOP mice are available upon request from the lead contact under an institutional MTA. All other reagents generated in this study and detailed protocols used in this study are available upon request from the lead contact.

Data and code availability

- 16S-V4 rRNA sequencing data have been deposited at NCBI BioProject database (http://www.ncbi.nlm.nih.gov/bioproject/) and are publicly available as of the date of publication. Accession numbers are listed in the key resources table.
- This paper does not report original code. References to all code used are available in the Method details section.
- Any additional information required to reanalyze the data reported in this paper is available from the lead contact upon request.

EXPERIMENTAL MODEL AND SUBJECT DETAILS

Animals

Mice were purchased from the Jackson Laboratories and bred (except for *Cd36*$^{-/-}$ mice) at Columbia University. Animals were purchased only from SFB-negative maximum barrier rooms at Jackson. All animals were tested for SFB upon arrival and maintained in

an SFB-negative high barrier room at Columbia University. 7B8 mice were bred to CD45.1 and IL-17-GFP mice at Columbia University to generate 7B8.CD45.1.IL-17-GFP animals. RORγ−STOP mice were generated by homologous recombination in C57BL/6 ES cells. The targeting vector generated an inversion of the *Rorc* genomic sequence containing Exons 3–6 surrounded by two pairs of *LoxP* and *LoxP*2272 sequences in opposite orientation in intron 2 and intron 6 (Figure S2). To generate ILC3-deficient mice that can generate CD4 T cells and Th17 cells, RORγ−STOP mice were crossed to *Cd4-Cre* mice. All mice were bred and housed under high-barrier specific pathogen-free conditions at Columbia University Irving Medical Center. Except for $Cd36^{-/-}$, all other lines were bred to heterozygocity and experiments were performed with littermate controls. Whenever possible all genotypes were housed in the same cage to control for microbiota and cage effects. $Cd36^{-/-}$ animals were ordered from the Jackson Laboratories with age and sex-matched C57BL/6J controls from the same room at Jackson and co-housed for two weeks prior to the start of the experiment and for the duration of the experiment to control for microbiota differences. Germ-free C57BL/6 mice were generated at the gnotobiotic facilities at Rockefeller University, Weill Cornell or Keio University and following defined flora colonization were housed in Techniplast isocages at the same institution. Metabolic experiments used 5-week-old males.

METHOD DETAILS

Diets

All diets were irradiated for sterility. Diets were provided in pellet form *ad libitum* and fresh diet provided twice a week. For 50:50 NCD:HFD mix, pellets from individual diets were mechanically disrupted into fine powder. 30 mg powder from each diet were mixed manually with 5–10 mL of autoclaved water to form a palatable pellet. The pellets were dried for 30 min and provided *ad libitum* to the animals on a clean plastic plate inside the cage. Fresh mixed diet pellets were provided twice weekly. Individual diet formulations are listed in Table S1.

Metabolic measurements

5-week-old males were colonized with SFB on Day −14 and kept on NCD. SFB colonization was confirmed on Day −10 and Day −1. On Day 0 the animals were switched to corresponding diets. Body weight was followed every 3–4 days throughout the experiment. Insulin tolerance test was performed on Day 28. Oral glucose tolerance test was performed on Day 32. Tissue and cell isolation for flow cytometry or quantitative RT-PCR was performed on Day 35. For insulin tolerance test, animals were subjected to a 6-h fast (8AM-2PM), followed by intraperitoneal insulin injection (0.75 U/kg, human insulin). Blood samples were obtained at 0, 20, 40, 60 and 120 min. For glucose tolerance test, animals were subjected to an overnight fast (6PM-6AM) followed by oral glucose gavage (1.2 g/kg of 12% dextrose solution). 2μL blood samples were obtained at 0, 15, 30, 60 and 120 min.

T cell and cytokine depletion *in vivo*

To deplete CD4 T cells *in vivo*, animals were injected intraperitoneally with an anti-CD4 antibody or isotype control twice weekly starting on Day 0. To neutralize IL-17A, 300 ug/mouse of an IL-17A neutralizing antibody or IgG1 isotype control were injected intraperitoneally every other day.

Adoptive T cell transfers

For adoptive transfer experiments, 0.5 million CD4 T cells (95%–98% purity) were MACS-purified from spleens and lymph nodes of SFB-negative 7B8/CD45.1/IL-17A-GFP reporter mice, labeled with Cell Trace Violet proliferation dye (Life Technologies) and transferred intravenously into congenic CD45.2 WT mice fed with corresponding diets. Priming and IL-17A induction in SI LP were investigated 7 days after transfer. For CD4 T cell reconstitution experiments, 5–10 million MACS purified CD4 T cells from spleens and LNs of SFB-negative WT/CD45.1/IL-17A-GFP reporter mice were transferred into recipient congenic STOP/CD45.2 mice.

Isolation of tissue for RNA preparation and quantitative RT-PCR

RNA was isolated from tissues after homogenization in Trizol using manufacturer's protocol. After cDNA synthesis, Q-PCR was performed on LightCycler 480 (Roche) using SYBR Green. Individual parts of the intestine were prepared as follows. Duodenum was dissected macroscopically. The remaining small intestine was divided into four equal parts and the parts were defined as proximal jejunum, distal jejunum, proximal ileum and distal ileum. For RNA isolation 0.5 cm tissue was collected from the center of the pieces defined as duodenum (Duo), distal jejunum (Jej) and distal ileum (Ile). Intestinal epithelial cells (IECs) were collected from the corresponding part of the small intestine by thorough washing of mucus with PBS followed by gentle scraping of the luminal surface with a glass slide.

Lamina propria lymphocyte isolation

LP lymphocytes isolation and intracellular cytokine and transcription factor staining were performed as described previously (Goto et al., 2014).

Adipose tissue immune cell isolation

Both flaps of epididymal fat were dissected and cut into small pieces. The sample was digested for 45 min at 37 °C with 2 mg/mL typeI collagenase and 1.5% FCS in RPMI.

Neutral lipid measurement

Neutral lipids were extracted using published protocol (Kraus et al., 2015) and measured with a commercial lipid quantification kit (see Key Resources Table).

Public RNA-seq data analysis

To examine if IL-17A acts on epithelial cells, previously reported RNA sequencing (RNA-seq) of mouse ileum enteroids (Kumar et al., 2016) and single-cell RNA sequencing (scRNA-seq) of total small intestine organoids (Biton et al., 2018) treated *in vitro* with rIL-17A or control were downloaded from NCBI Sequence Read Archive (SRA). For bulk RNA-seq, single-ended raw reads were processed by Cutadapt v2.1 (reference) with following parameters "–minimum-length 24 -u 10 –trim-n -q 15" to remove low-quality bases and Illumina adapters. Reads passing quality filtering were then aligned against mouse cDNA reference GRCm38 by Bowtie2 v2.3.4 (Langmead and Salzberg, 2012) in –very-sensitive mode and reads counts per gene were then normalized by gene length and sequencing depth, i.e., reads per kilobase per million mapped reads (RPKM), for expression level quantification. For scRNAseq, raw reads were processed by 10X Genomics Cellranger toolkit v1.0.1 according to the original paper. Next, cells with fewer than 500 detected genes were excluded, and remaining cells were subjected to UMAP ordination and clustering following standard Seurat pipeline (Hao et al., 2021). Cell types were manually identified by top cluster markers and gene expression level was calculated by function "AverageExpression" implemented in Seurat package.

Bacterial strains

SFB were obtained from feces of SFB-monocolonized mice housed at Keio University. *Faecalibaculum rodentium (Frod)* (PB1) and *Bifidobacterium pseudolongum (Bpl)* (1B11) were isolated in the Kenya Honda laboratory (RIKEN IMS) as previously described (Atarashi et al., 2015; Zagato et al., 2020). *B. pseudolongum* was chosen as a control strain for *Frod* gnotobiotic experiments, because it is a relatively high abundance species in our mouse colony that further increased after treatment with sucrose, but not with HFD. *Frod* and *Bpl* cultures were grown in pre-reduced Eggerth-Gagnon (EG) medium (*Frod*) or Reinforced Clostridial Medium (Fisher DF1808-17-3) (*Bpl*) in an anaerobic chamber (5% H_2, 10% CO_2, 85% N_2) at 37C for 48 h. For *Frod* colonization, mice were gavaged with 200 μL of overnight culture resuspended in pre-reduced PBS (optical density (OD) 600 ≅ 0.6; corresponding to about 5×10^7 cfu/mL. For colonization of SPF mice, WT or STOP/CD4 recipient animals were pre-treated with 1 g/L ampicillin in the drinking water for four days. For *Bpl* colonization, animals received 1×10^8 cfu/mL of 1B11 in 200 μL pre-reduced PBS by oral gavage.

SFB colonization and relative SFB quantification

Unless otherwise noted, SFB colonization was performed 2 weeks prior to diet change by single oral gavage of fecal suspension from SFB-enriched mice as previously described (Farkas et al., 2015). For SFB probiotic treatment, animals were gavaged every other day. Control animals were gavaged with fecal suspensions from SFB-negative littermate controls. To control for variability in SFB levels in feces used for gavage, all gavages were performed with frozen stocks from a single batch of SFB-enriched feces. To generate SFB-enriched feces a single cohort of 10 adult SFB-negative maximum barrier NSG mice from The Jackson Laboratory were colonized with feces from SFB-monocolonized mice. Fecal samples were obtained in the period of 8 weeks, tested for SFB by quantitative RT-PCR and frozen as batch aliquots at −80C. Control SFB-negative feces were collected from a separate cohort of littermate NSG mice housed in a similar manner. SFB colonization levels were confirmed by qPCR and normalized to levels of total bacteria (UNI) as previously described (Farkas et al., 2015).

Absolute quantification of bacterial species in feces

Absolute levels of SFB, *Faecalibaculum rodentium* (*Frod*) and *B. pseudolongum (Bpl)* were measured by quantitative RT-PCR and quantified as μg of DNA per gram feces using standard curves from mono-colonized mice (SFB) or *in vitro* culture (*Frod, Bpl*).

Fecal bacterial DNA extraction and 16S rRNA amplicon sequencing

Genomic DNA from feces was extracted using a silica bead beating-based protocol as previously described (Farkas et al., 2015). 16S sequencing of the V4 region was performed utilizing a custom dual-indexing protocol, detailed fully in (Ji et al., 2019).

OTU clustering and absolute abundance calculation

Raw sequencing reads of 16S-V4 amplicons were analyzed by USEARCH v11.0.667 (Edgar, 2010). Specifically, paired-end reads were merged using "-fastq_mergepairs" mode with default setting. Merged reads were then subjected to quality filtering using "--fastq_filter" mode with the option "-fastq_maxee 1.0 -fastq_minlen 240". Remaining reads were deduplicated (-fastx_uniques) and clustered into OTUs (-unoise3) at 100% identity, and merged reads were then searched against OTU sequences (-otutab) to generate OTU count table. Taxonomy of OTUs were assigned using RDP classifier trained with 16S rRNA training set 18 (Wang et al., 2007). Sample total bacterial loads were calculated based on reads ratio of spike-in strain and sample weight, and relative abundance profiles of other taxa were then scaled by bacterial load to obtain absolute OTU abundances in arbitrary units, detailed fully in (Ji et al., 2019).

Public human feces shotgun metagenome data analysis

To examine if Th17-inducing gut microbiota were altered under different conditions, two previously reported metagenome datasets from feces (metabolic syndrome versus healthy controls (Pedersen et al., 2016) and healthy individuals with recorded diet (Johnson et al., 2019)) were downloaded from NCBI Sequence Read Archive (SRA). Reference genomes of 20 Th17-inducing gut strains (Atarashi et al., 2015) were accessed according to the original paper and reference genomes of *B. adolescentis* and *E. lenta* were downloaded from NCBI Genome under accession NZ_CP028341.1 and NZ_CP089331.1. Reads of each sample were processed by Cutadapt v2.1 (Martin, 2011) with following parameters "–minimum-length 24:24 -u 5 -U 5 -q 20 –pair-filter = any" to remove low-quality bases and Nextera adapters. Reads passing quality filtering were then aligned against reference genomes by Bowtie2 v2.3.4 (Langmead and Salzberg, 2012) in –very-sensitive mode and relative abundances of each strain were calculated as # of reads mapped to the strain normalized by total reads count. For the dataset of metabolic syndrome versus healthy control, 295 non-diabetic individuals were classified into "with metabolic syndrome" and "without metabolic syndrome" according to individual annotations in the original paper (Pedersen et al., 2016). For the community of 20 Th17-inducing strains, high depletion was defined as more than 12 strains showing less than 25th percentile relative abundance across all individuals. For the dataset of recorded diet, index of "L2: sugar and sweets" in dietary records were extracted from the original paper (Johnson et al., 2019) and 509 samples from 34 individuals with accessible shotgun metagenome data were classified into high and low "Sugar and sweets consumption" using threshold of 25 for "L2: sugar and sweets" index.

Electron microscopy

SFB-monocolonized mice were inoculated with *Frod* and samples from the terminal ileum were extracted after 24 h and processed for electron microscopy as previously described (Ladinsky et al., 2019). Semi-thin (170 nm) sections were cut with a UC6 ultramicrotome (Leica Microsystems, Vienna), stained with uranyl acetate and lead citrate, and imaged on a Tecnai T12 transmission electron microscope (Thermo-Fisher Scientific) at 120k eV.

QUANTIFICATION AND STATISTICAL ANALYSIS

Unless otherwise noted, statistical significance was determined by one-way ANOVA for panels where more than three groups are being compared, and unpaired t test with Welch's correction for panels where two groups are compared. p values are represented on figures as follows: ns, not significant, *$p < 0.05$, **$p < 0.01$, ***$p < 0.005$, ****$p < 0.001$, *****$p < 0.0005$. On time course panels, p values with a bracket line connecting two curves refer to the whole curves and p values on top of individual datapoints refer only to those individual datapoints. Error bars on all figures represent standard deviation of the mean. Statistical analysis was performed using GraphPad Prism version 9.0 for Windows (GraphPad Software).

Supplemental figures

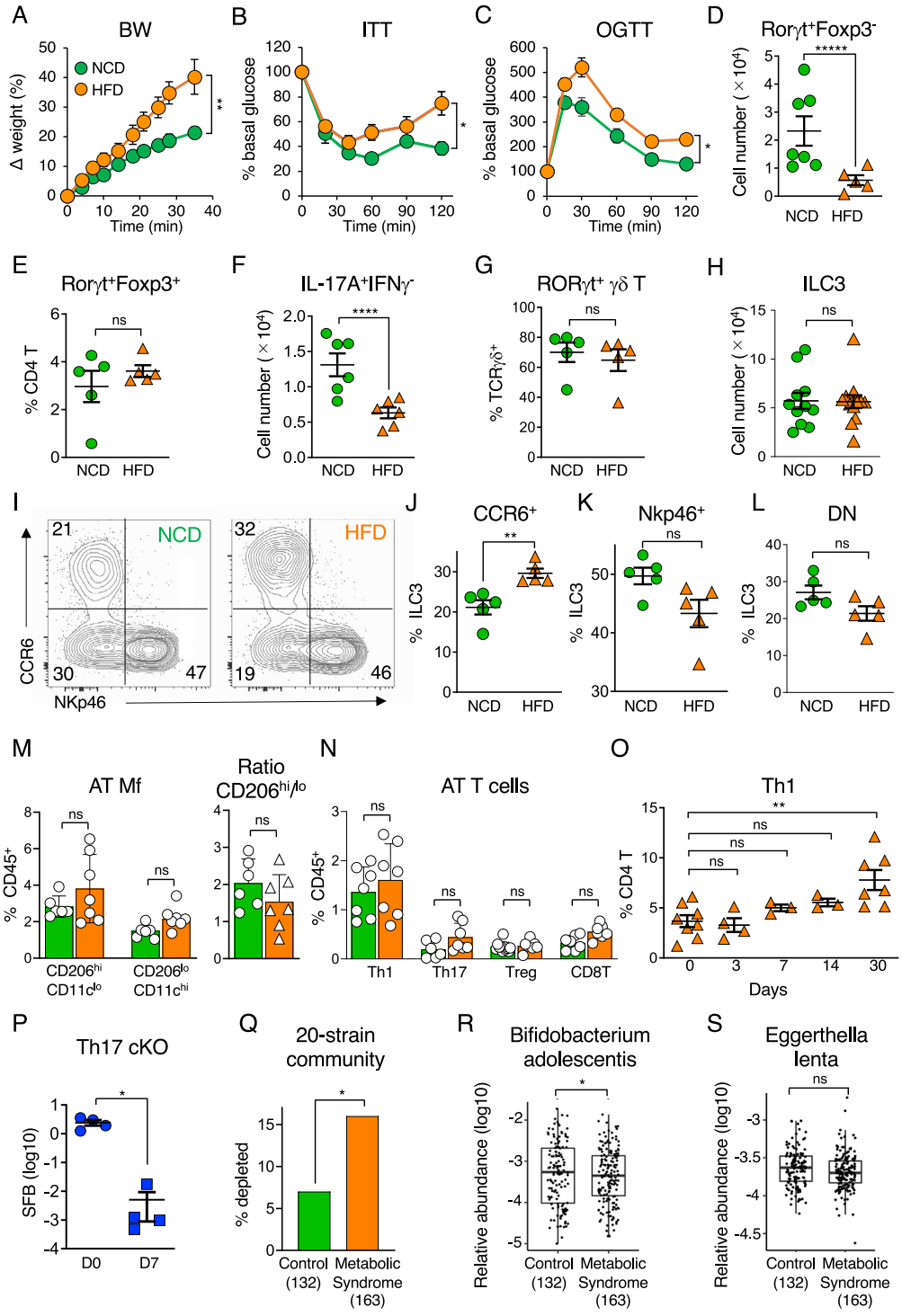

(legend on next page)

Figure S1. HFD disrupts intestinal immune homeostasis by eliminating Th17-inducing microbiota, related to Figure 1

(A–C) Metabolic analyses at 5 weeks on high-fat diet (HFD) vs normal chow (NCD). Data from two out of multiple independent experiments.

(D–G) Flow cytometry of SI LP CD4 T cells in WT C57BL/6 mice fed with NCD or HFD for 4 weeks. Plots gated on TCRβ^+CD4$^+$ lymphocytes. Data from two out of multiple independent experiments, n = 7 mice/group.

(H–L) Flow cytometry analysis of ILC3 (Lin^{neg}RORγt$^+$) and ILC3 subsets in SI LP of WT C57BL/6 mice fed NCD or HFD for 5 weeks. Data from two out of multiple independent experiments, n = 5–11 mice/group.

(M and N) Flow cytometry analysis of (M) macrophage (Mf) and (N) T cell subsets in visceral adipose tissue (AT) of WT C57BL/6 mice fed NCD or HFD for 4 weeks. Plots gated on CD45$^+$ hematopoietic cells. Data from one experiment, n = 7 mice/group.

(O) Time course of the proportion of Th1 cells within SI LP CD4 T cells in WT C57BL/6 mice fed HFD. Data combined from two independent experiments, n = 4–8 mice/group.

(P) SFB levels in feces of RORγt-flox/CD4-Cre (Th17 cKO) mice before (D0) and 7 days after (D7) transition to HFD. Data from one out of two independent experiments, n = 3–4 mice/group.

(Q) Proportion of individuals showing high depletion in 20 Th17-inducing gut strains (Atarashi et al., 2015) in metabolic syndrome (*N* = 163) versus control group (*N* = 132) (metagenomic data from Pedersen et al., 2016).

(R and S) Relative abundance of previously reported Th17-inducing gut strains, (R) *Bifidobacterium adolescentis* and (S) *Eggerthella lenta* in metabolic syndrome (*N* = 163) versus control group (*N* = 132) (metagenomic data from Pedersen et al., 2016).

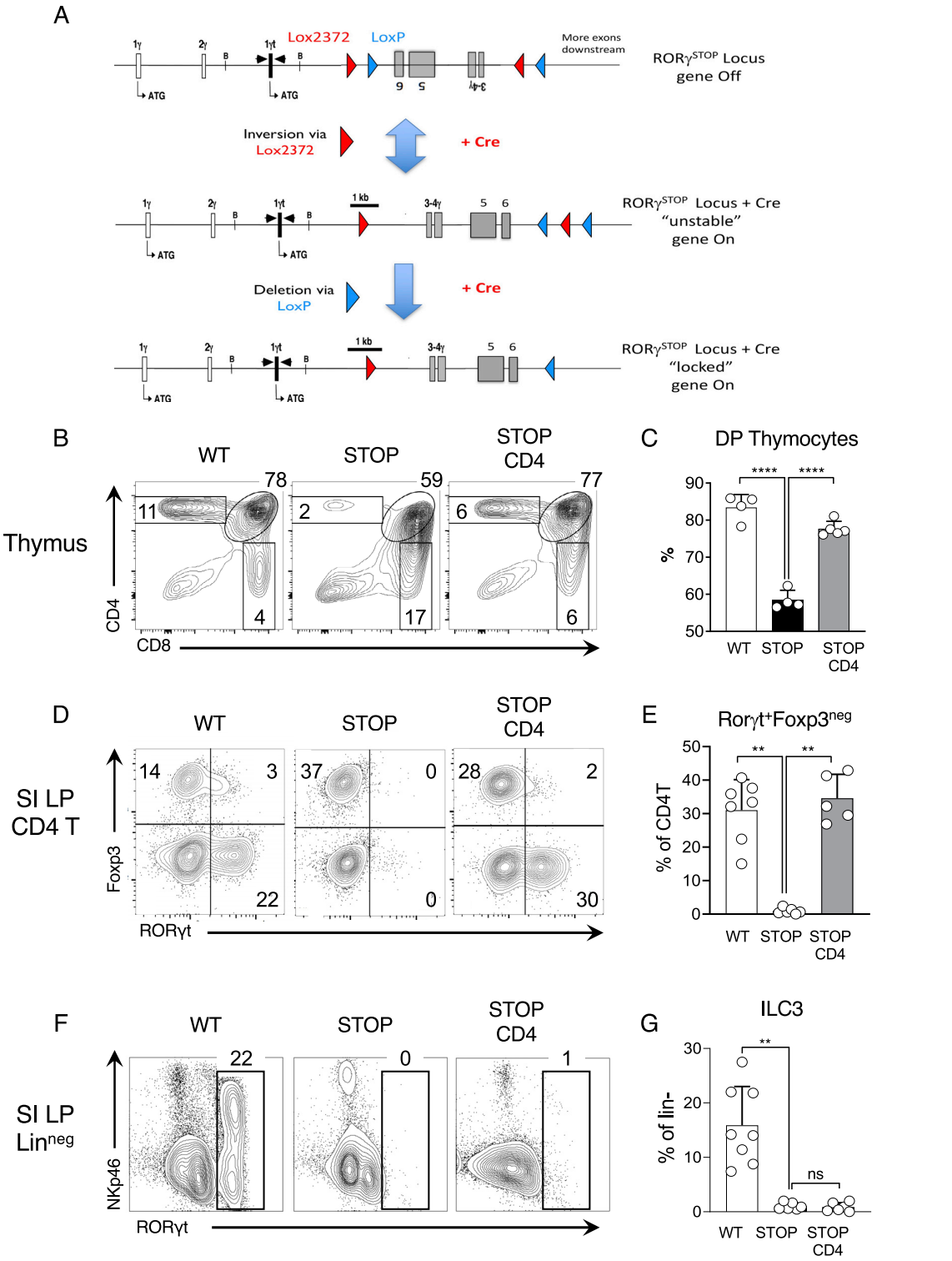

(legend on next page)

Figure S2. Generation of ILC3-deficient, Th17 cell-sufficient mice, related to Figure 2

(A) Scheme of genetic modifications for generation of RORγ-STOP mice.

(B and C) Recovery of thymocyte development in RORγ-STOP/CD4-Cre (STOP/CD4) mice. (C) double-positive (DP) thymocytes. Data from one out of multiple independent experiments, n = 5 mice/group.

(D and E) Recovery of small intestinal RORγ^{+} Th17 cells (E) and RORγ^{+}Foxp3^{+} Tregs in STOP/CD4 mice. Plots gated on TCRβ^{+}CD4^{+} cells. Data from two out of multiple independent experiments, n = 5–7 mice/group.

(F and G) Lack of small intestinal ILC3 in STOP/CD4 mice. Plots in (F) gated on Lin^{neg} cells (TCRβ^{neg}CD3^{neg}B220^{neg}). Data from two out of multiple independent experiments, n = 5–7 mice/group.

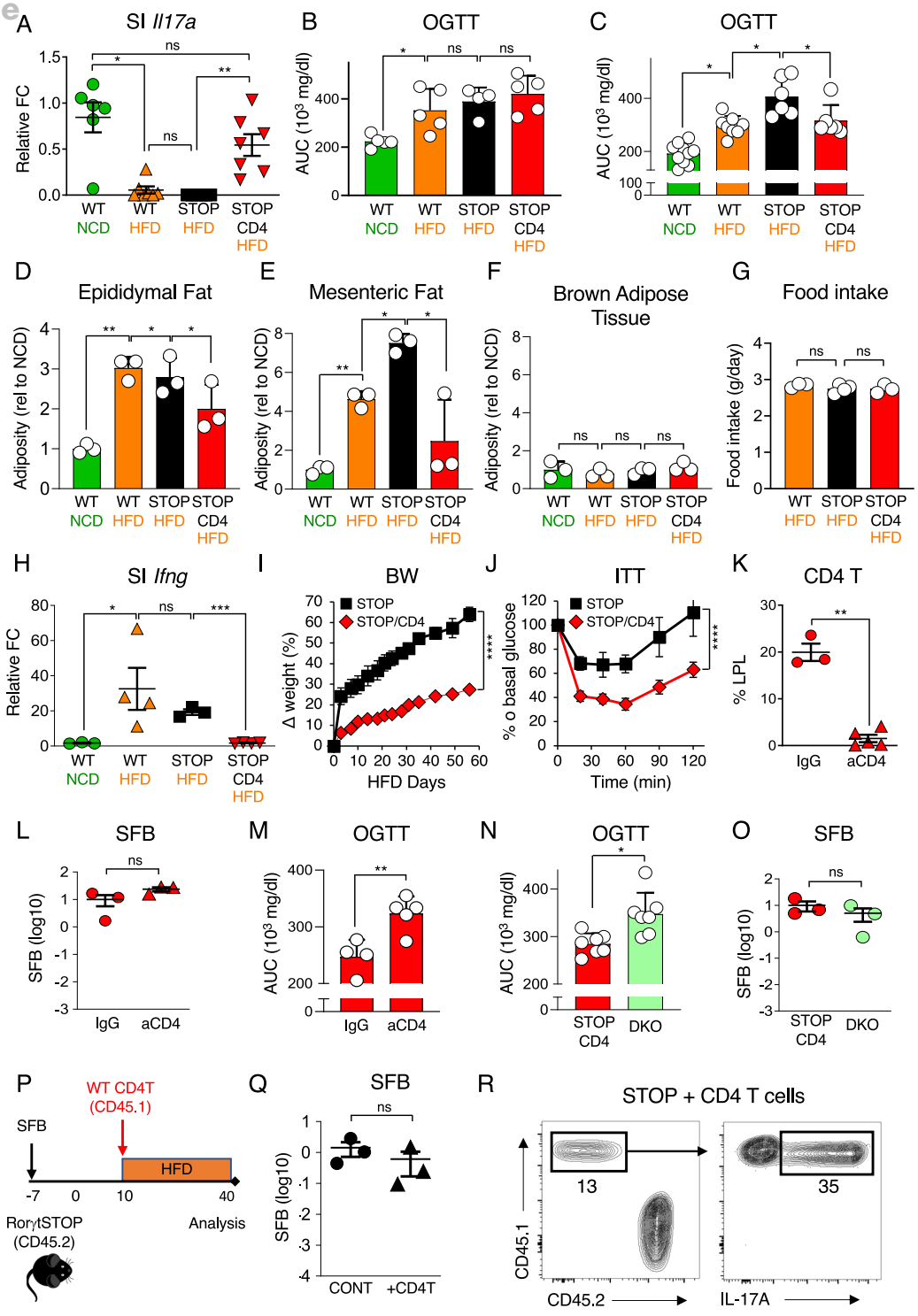

Figure S3. Microbiota-induced Th17 cells protect from metabolic syndrome, related to Figure 2

(A) Quantitative RT-PCR for *Il17a* transcripts in terminal ileum tissue samples from WT, STOP and STOP/CD4 mice fed NCD or HFD for 5 weeks. Data combined from two independent experiments, n = 6–8 mice/group.

(B and C) Glucose tolerance test of (B) SFB-negative and (C) SFB-positive WT, STOP and STOP/CD4 mice after 5 weeks on NCD or HFD. Data from two (B) and three (C) out of multiple independent experiments, n = 5–10 mice/group.

(legend continued on next page)

(D–F) Adiposity in (D) epididymal fat, (E) mesenteric fat and (F) brown adipose tissue of WT mice on NCD, of HFD-fed WT, STOP, or STOP/CD4 mice. Data from one out of two independent experiments, n = 3 mice/group.
(G) Daily food intake in HFD-fed WT, STOP, and STOP/CD4 mice. Data from one out of two independent experiments, n = 4 mice/group.
(H) Quantitative RT-PCR for *Ifng* transcripts in terminal ileum samples from WT, STOP and STOP/CD4 mice fed HFD for 5 weeks. Data combined from two independent experiments, n = 3–4 mice/group.
(I and J) Metabolic analyses at 8 weeks of SFB-positive HFD-fed STOP and STOP/CD4 mice. One experiment, n = 5 mice/group.
(K–M) CD4 T cells in SI LP (K), SFB levels in feces (L) and glucose tolerance test (M) of STOP/CD4 mice treated with anti-CD4 mAb to deplete CD4 T cells or isotype control (IgG) and fed HFD for 5 weeks. Data combined from two independent experiments, n = 3–5 mice/group.
(N and O) Glucose tolerance test (N) and SFB levels in feces (O) of STOP/CD4 and STOP/CD4 TCRβ-deficient double knock-out (DKO) mice fed HFD for 5 weeks. Data from two independent experiments, n = 7 mice/group.
(P–R) Transfer of WT CD4 T cells in ILC3/Th17-deficient STOP mice. (P) Experimental design, (Q) SFB levels in feces and (R) transferred Th17 cells in SI LP five weeks after transfer. Data from one out of two independent experiments, n = 5 mice/group.
AUC, area under curve.

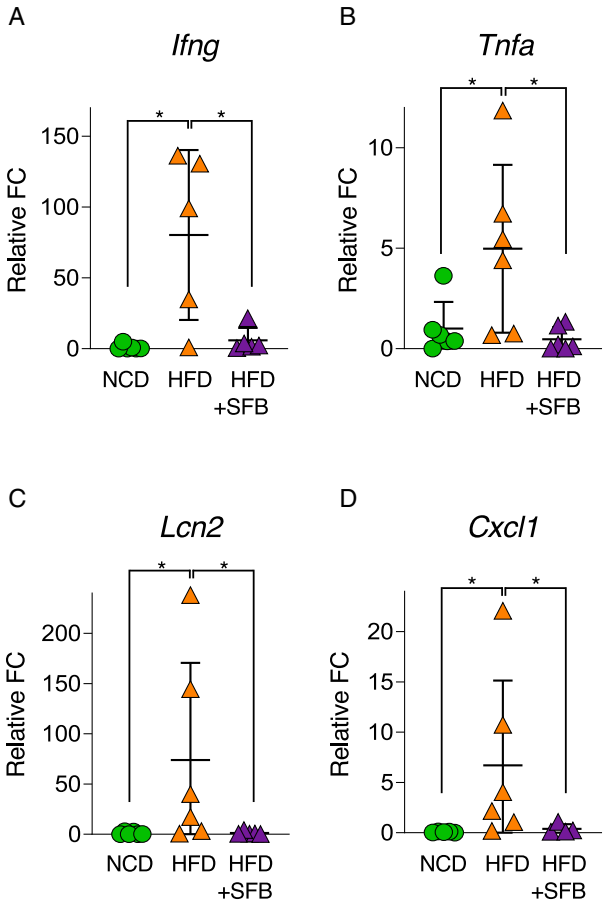

Figure S4. Probiotic Th17 cell-inducing bacteria ameliorate metabolic syndrome, related to Figure 3

(A–D) Quantitative RT-PCR of (A) *Ifng,* (B) *Tnfa,* (C) Lipocalin (*Lcn2),* and (D) *Cxcl1* transcripts in terminal ileum at 4 weeks. Data from two independent experiments, n = 6 mice/group.

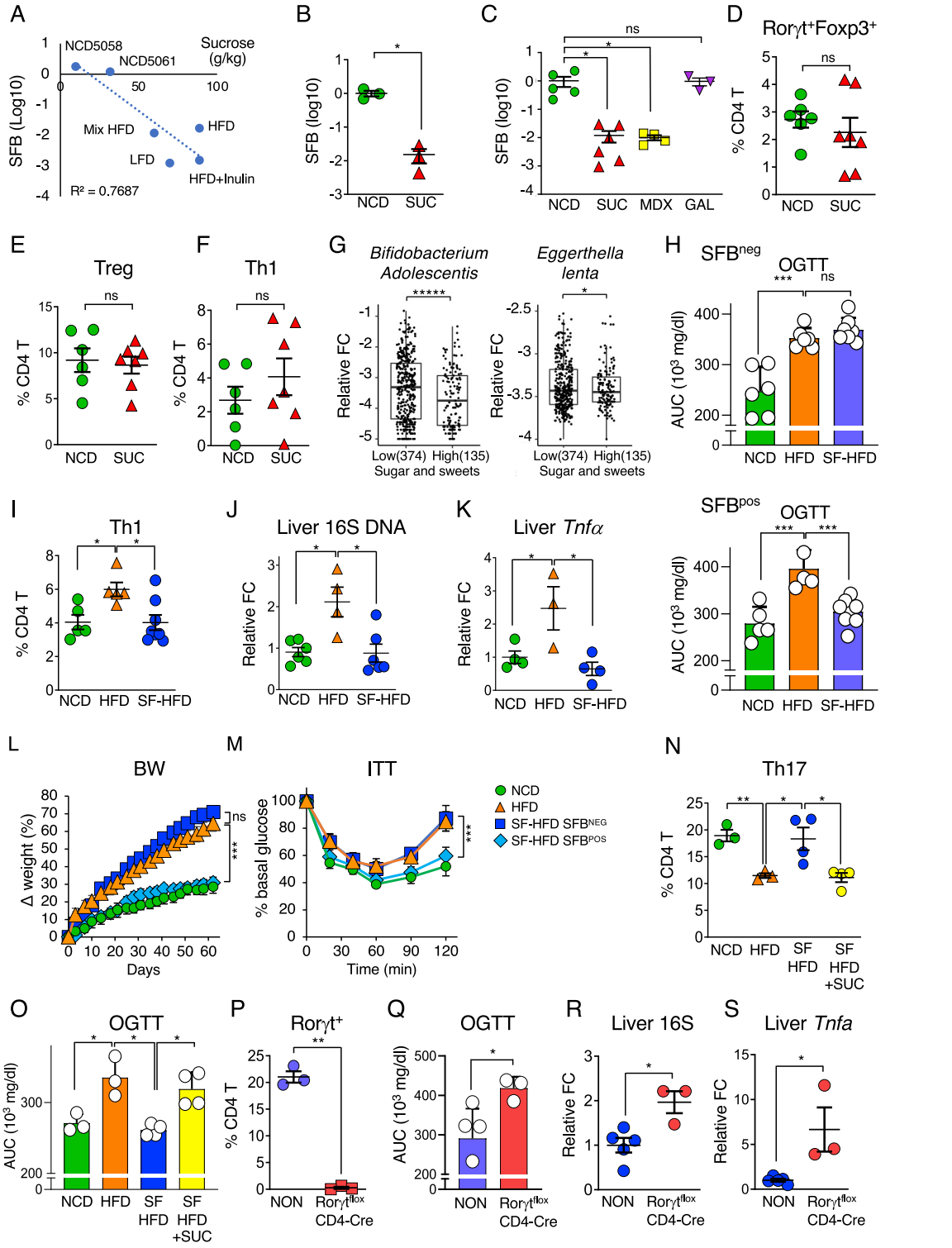

(legend on next page)

Figure S5. Dietary sugar promotes metabolic syndrome through elimination of commensal Th17 cells, related to Figure 4

(A) Correlation between sucrose content in various diets and fecal SFB levels in WT C57BL/6 mice after 1 week on the corresponding diet.

(B) qPCR of SFB levels in terminal ileum mucosa of WT C57BL/6 mice fed natural gradient normal chow diet (NCD) or NCD +10% sucrose in the drinking water (SUC) for 1 week. Data from one out of two independent experiments, n = 3 mice/group.

(C) qPCR of SFB in feces of WT C57BL/6 mice fed NCD or NCD plus various sugars for one week. SUC, sucrose; MDX, maltodextrin; GAL, galactose. All sugars were provided at 10% w/v in the drinking water. Data from two independent experiments, n = 3–7 mice/group.

(D–F) RORγt^{+} (D) and RORγt^{neg} (E) Foxp3^{+} Tregs and IFNγ^{+} Th1 cells (F) in SI LP of mice fed NCD or NCD plus 10% sucrose in the drinking water (SUC) for 1 week. Data from two out of multiple independent experiments, n = 6–7 mice/group.

(G) Relative abundance of previously reported Th17-inducing gut strains, *Bifidobacterium adolescentis* and *Eggerthella lenta* in shotgun metagenomic sequencing data (Johnson et al., 2019) from healthy volunteers with low or high sugar consumption (details in STAR Methods).

(H) Oral glucose tolerance test (OGTT) on Day 35 in SFB-negative (top) or SFB-colonized (bottom) WT C57BL/6 mice fed NCD, HFD, or sugar-free HFD (SF-HFD). Data from two independent experiments, n = 5–7 mice/group

(I) Th1 cells in SI LP of SFB-gavaged WT C57BL/6 mice fed NCD, HFD, or sugar-free HFD (SF-HFD). Data represented as proportion of TCRβ^{+}CD4^{+} cells on Day 40. Data from two out of multiple independent experiments, n = 5–9 mice/group.

(J and K) qPCR for total bacterial 16S DNA (L) and quantitative RT-PCR for *Tnf*α transcripts in liver of SFB-gavaged WT C57BL/6 mice fed NCD, HFD, or sugar-free HFD (SF-HFD) for 5 weeks. Data from two independent experiments, n = 4–6 mice/group.

(L and M) Metabolic phenotypes of SFB-negative or SFB-colonized C57BL/6 mice fed indicated diets for 9 weeks. Data from one experiment, n = 5 mice/group.

(N) Th17 cells in SI LP of SFB-colonized WT C57BL/6 mice fed NCD, HFD, SF-HFD, or SF-HFD supplemented with 10% sucrose (+SUC) in the drinking water for 5 weeks. Data from two independent experiments, n = 3–5 mice/group.

(O) Oral glucose tolerance test (OGTT) of SFB-colonized WT C57BL/6 mice fed NCD, HFD, SF-HFD, or SF-HFD supplemented with 10% sucrose (+SUC) in the drinking water for 5 weeks. Data from two independent experiments, n = 3–5 mice/group.

(P and Q) Th17 cells (RORγt^{+} CD4 T cells) (P) and oral glucose tolerance test (Q) of SFB-colonized Th17 cell-deficient RORγt$^{flox/flox}$,CD4-Cre mice and control littermates fed SF-HFD for 5 weeks. Data from one out of two independent experiments, n = 3–5 mice/group.

(R and S) qPCR for total bacterial 16S DNA (R) and quantitative RT-PCR for *Tnf*α transcripts (S) in liver of SFB-colonized Th17 cell-deficient RORγt$^{flox/flox}$,CD4-Cre mice and control littermates fed SF-HFD for 5 weeks. Data from two independent experiments, n = 5 mice/group.

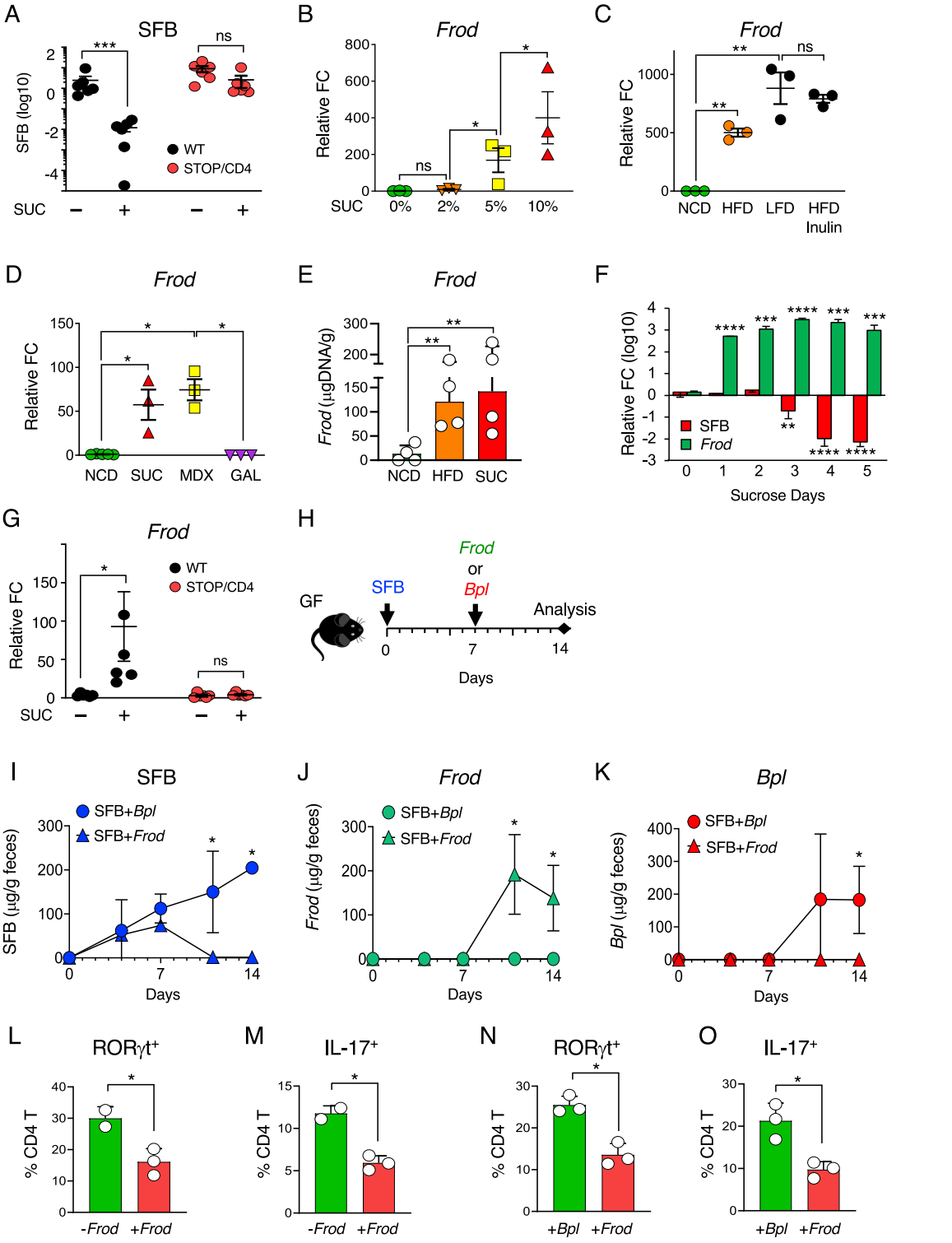

(legend on next page)

Figure S6. Dietary sugar displaces Th17 microbiota by increasing *Faecalibaculum rodentium*, related to Figures 5 and 6

(A) qPCR of SFB in feces of WT and ILC3-deficient/Th17-sufficient STOP/CD4 mice before and 7 days after treatment with 10% sucrose (SUC) in the drinking water. Data from two independent experiments, n = 6 mice/group

(B) qPCR of *Frod* in feces of WT mice on NCD or NCD plus various concentration of sucrose (SUC) in drinking water. Data plotted as relative fold change (FC) over NCD group. Data from one experiment, n = 3 mice/group.

(C) qPCR of *Frod* in feces of WT mice fed NCD, HFD, LFD and HFD + Inulin for 1 week. Data plotted as relative fold change (FC) over NCD group. Data from one out of two independent experiments, n = 3 mice/group.

(D) qPCR data of *Frod* in feces of WT mice on NCD or NCD plus various types of sugars for one week. SUC, sucrose; MDX, maltodextrin; GAL, galactose. All sugars were provided at 10% w/v in the drinking water. Data plotted as relative fold change (FC) over NCD group. Data from two independent experiments, n = 3–7 mice/group.

(E) qPCR of *Frod* in feces of SFB-negative WT mice fed indicated diets for 1 week. Data from one out of two independent experiments, n = 4 mice/group.

(F) Kinetics of SFB and *Frod* in feces of WT mice on NCD following addition of 10% sucrose in the drinking water. Data plotted as relative fold change (FC) over NCD group. Data from one experiment, n = 3 mice/group.

(G) qPCR of *Frod* in feces of SFB-positive WT and ILC3-deficient/Th17-sufficient STOP/CD4 mice before and 7 days after treatment with 10% sucrose (SUC) in the drinking water. Data plotted as relative fold change (FC) over WT No sucrose group. Data from two independent experiments, n = 6 mice/group.

(H–K) *Frod* is sufficient to displace SFB. (H) Experiment scheme. Germ-free C57BL/6 mice were colonized by oral gavage with SFB and a week later with either *Frod* or *Bifidobacterium pseudolongum* (*Bpl*).

(I–K) Levels of the three microbes were followed in feces by qPCR for two weeks. Data from one experiment, n = 3 mice/group.

(L and M) RORγt^{+}Foxp3^{neg} (L) and IL-17^{+} (M) Th17 cells in the SI LP of GF animals colonized first with SFB and then with or without *Frod* as per the experimental scheme on Figure 6G. Mice were analyzed 7 days post *Frod* gavage. Data presented as proportion of TCRβ^{+}CD4^{+} cells. Data from one out of two independent experiments, n = 2–3 mice/group.

(N and O) RORγt^{+}Foxp3^{neg} (N) and IL-17^{+} (O) Th17 cells in the SI LP of gnotobiotic mice colonized with SFB and other bacteria. All animals were first colonized with SFB, followed by gavage with *Frod* or *Bifidobacterium pseudolongum* (*Bpl*) a week later as per the scheme on Figure S6H. Mice were analyzed 7 days post *Frod*/*Bpl* gavage. Data presented as proportion of TCRβ^{+}CD4^{+} cells. Data from one experiment, n = 3 mice/group.

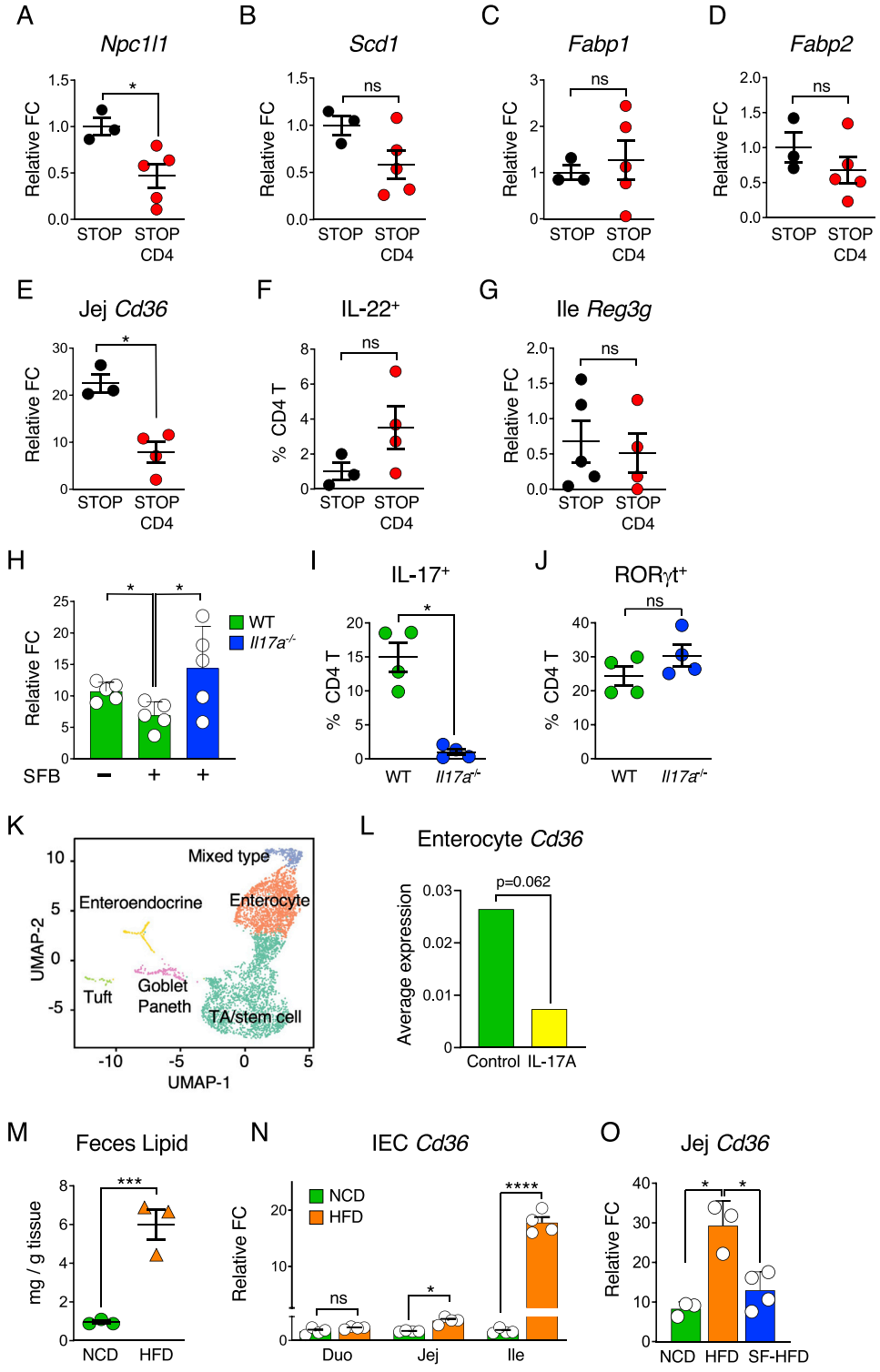

(legend on next page)

Figure S7. Commensal Th17 cells prevent metabolic syndrome by regulating intestinal lipid absorption, related to Figure 7

(A–D) Quantitative RT-PCR for transcripts of lipid transporters in ileum IECs from SFB-positive Th17-deficient STOP and Th17-sufficient STOP/CD4 mice fed HFD for 5 weeks. Data from two independent experiments, n = 3–5 mice/group.

(E) Quantitative RT-PCR for *Cd36* transcripts in jejunum IECs from SFB-positive STOP and STOP/CD4 mice fed HFD for 5 weeks. Data from two independent experiments, n = 3–5 mice/group.

(F) IL-22$^+$ CD4 T cells in the SI LP of STOP and STOP/CD4 mice fed HFD for 5 weeks. Data from two independent experiments, n = 3–4 mice/group.

(G) Quantitative RT-PCR of transcripts for the IL-22-induced IEC gene *Reg3g* in total ileum from STOP and STOP/CD4 mice fed HFD for 5 weeks. Data from two independent experiments, n = 4 mice/group.

(H) Quantitative RT-PCR for *Cd36* transcripts in jejunum IECs from WT and IL-17A-deficient mice. Data from two independent experiments, n = 5 mice/group.

(I and J) IL-17A$^+$ (I) and RORγt$^+$ (J) Th17 cells in SI LP of SFB-positive IL-17A-deficient mice. Data from two independent experiments, n = 4–5 mice/group.

(K and L) Small intestinal enteroids were treated with rIL-17A *in vitro* (analysis of scRNA-Seq data from Biton et al., 2018). (K) Ordination of profiled single cells by UMAP. (L) Expression level of *Cd36* in the enterocyte cluster under different conditions. Statistics (L), Mann-Whitney U test.

(M) Total neutral lipid contents in feces of SFB-negative WT C57BL/6 mice fed NCD or HFD for 4 weeks. Data from one experiment, n = 3 mice/group.

(N) Quantitative RT-PCR for *Cd36* transcripts in IECs from duodenum (Duo), jejunum (Jej) and ileum (Ile) of SFB-negative WT C57BL/6 mice fed NCD or HFD for 5 weeks. Data from two independent experiments, n = 4 mice/group.

(O) Quantitative RT-PCR for *Cd36* transcripts in IECs from jejunum (Jej) of SFB-gavaged WT C57BL/6 mice fed with indicated diets for five weeks. Data from one experiment, n = 4 mice/group